THE ASTROPHYSICAL JOURNAL, 460:489–505, 1996 March 20

ON THE EVOLUTION OF STARS THAT FORM ELECTRON-DEGENERATE CORES PROCESSED BY CARBON BURNING. II. ISOTOPE ABUNDANCES AND THERMAL PULSES IN A 10 $M_\odot$ MODEL WITH AN ONe CORE AND APPLICATIONS TO LONG-PERIOD VARIABLES, CLASSICAL NOVAE, AND ACCRETION-INDUCED COLLAPSE[1]

CLAUDIO RITOSSA,[2,4] ENRIQUE GARCÍA-BERRO,[3] AND ICKO IBEN, JR.[4]
Received 1995 August 11; accepted 1995 September 27

ABSTRACT

A 10 $M_\odot$ model of Population I composition is evolved from the hydrogen-burning main sequence to the thermally pulsing "super"–asymptotic giant branch (TPSAGB) stage, where it has an oxygen-neon (ONe) core of mass 1.196 $M_\odot$ and is experiencing thermal pulses driven by helium-burning thermonuclear flashes. Interior abundance characteristics are relevant to an understanding of the core collapse of massive accreting white dwarfs in close binary star systems. At mass point 0.2 $M_\odot$, abundances by mass are $X(^{16}\mathrm{O}) = 0.656$, $X(^{20}\mathrm{Ne}) = 0.215$, $X(^{23}\mathrm{Na}) = 0.0467$, $X(^{24}\mathrm{Mg}) = 0.0325$, $X(^{25}\mathrm{Mg}) = 0.0115$, $X(^{12}\mathrm{C}) = 0.0112$, $X(^{22}\mathrm{Ne}) = 0.00893$, $X(^{21}\mathrm{Ne}) = 0.00689$, $X(^{26}\mathrm{Mg}) = 0.00560$, and $X(^{27}\mathrm{Al}) = 0.00528$. Abundances near the surface of the core are relevant to an understanding of nova outbursts in cataclysmic variables. At mass point 1.17 $M_\odot$, abundances by mass are $X(^{16}\mathrm{O}) = 0.511$, $X(^{20}\mathrm{Ne}) = 0.313$, $X(^{23}\mathrm{Na}) = 0.0644$, $X(^{24}\mathrm{Mg}) = 0.0548$, $X(^{25}\mathrm{Mg}) = 0.0158$, $X(^{27}\mathrm{Al}) = 0.0108$, $X(^{12}\mathrm{C}) = 0.00916$, $X(^{26}\mathrm{Mg}) = 0.00989$, $X(^{21}\mathrm{Ne}) = 0.00598$, and $X(^{22}\mathrm{Ne}) = 0.00431$. Carbon burning is quenched at the beginning of the thermally pulsing phase, and a layer of CO matter of mass ~ 0.015 $M_\odot$ separates the ONe core from overlying helium- and hydrogen-rich layers. The outer 0.01 $M_\odot$ of the CO layer contains essentially no neon: very little new ^{20}Ne has been made, and most of the ^{22}Ne which has been made from the original CNO elements has been converted into ^{25}Mg and neutrons which have been captured to form neutron-rich isotopes. If the observational counterpart of the model is in a close binary and fills its Roche lobe near the end of the carbon-burning phase, and if the binary evolves into a cataclysmic variable, one expects that the ejecta of approximately 1000 nova outbursts will exhibit an underabundance of neon and overabundance of carbon, oxygen, and magnesium.

During the TPSAGB phase, characteristics of a pulse cycle approach local limit-cycle values after ~ 30 pulses. Helium-shell flashes are of about the same strength ($L_{\mathrm{He}}^{\mathrm{max}} \sim 3 \times 10^6$ $L_\odot$, $L_{\mathrm{He}}^{\mathrm{min}} \sim 100$ $L_\odot$) as in AGB models with CO cores of mass ~ 1 $M_\odot$, but the time between flashes (~ 200 yr) and the mass of helium fuel built up between flashes ($\sim 1.3 \times 10^{-4}$ $M_\odot$) are much smaller. The amount of energy released in a flash is not enough to propel matter at the hydrogen-helium discontinuity far enough outward that associated cooling extinguishes hydrogen burning ($L_{\mathrm{H}}^{\mathrm{min}} \sim 10^2$ $L_\odot$, $L_{\mathrm{H}}^{\mathrm{max}} \sim 6 \times 10^4$ $L_\odot$). The temperature at the base of the convective shell forced by helium burning attains a maximum of $T_{\mathrm{CSB}}^{\mathrm{max}} \sim 360 \times 10^6$ K. Depending on the choice of cross section for the $^{22}\mathrm{Ne}(\alpha, n)^{25}\mathrm{Mg}$ reaction, 50%–80% the ^{22}Ne initially in the convective shell is converted into ^{25}Mg, providing 20–30 neutrons for every ^{56}Fe seed nucleus. The neutron density ($\sim 6 \times 10^{12}$ cm^{-3}) is presumably much larger than is appropriate for producing *s*-process isotopes in the solar system distribution at critical branch points. During pulse powerdown, at least 7% and perhaps as much as 30% of the matter which has been in the convective shell is dredged up into the convective envelope. Thus, an observational counterpart of the model may exhibit an enhancement of heavy *s*-process isotopes in a nonsolar distribution and Mg isotopes in a distinctly nonsolar distribution, but because of the large mass of the convective envelope, these anomalies may not be detectable in a typical TPSAGB star. The abundance of Li relative to H in a model may be much larger or much smaller than Li/H $\sim 10^{-10}$, depending on the treatment of convection and on where the model is in the TPSAGB phase. At the beginning of the TPSAGB phase, the surface abundances by number of CNO elements are in the ratio (C:N:O) = (2.4:4.3:6.3), compared with the initial ratios (C:N:O) = (3.6:1.0:8.0). During the TPSAGB phase, the ratio of C to N decreases, and the ratio of ^{12}C to ^{13}C decreases from ~ 25 to ~ 4. A test of these predictions involves abundance estimates of the brightest long-period variables in the Galaxy and in the Magellanic Clouds. Perhaps the major signature of a TPSAGB star is a brightness greater than the "classical limit" of $M_{\mathrm{bol}} = -7.1$. Betelgeuse in our Galaxy and four stars in the Magellanic Clouds are brighter than the supposed limit, but they exhibit abundance characteristics which can be accounted for in the framework of TPSAGB theory. Assuming that a superwind removes mass from the surface at a rate of $\sim 10^{-4}$ $M_\odot$ yr^{-1}, the final mass of the ONe

[1] Supported in part by the NSF (US) grants AST 91-13662 and AST 94-13662 and AST 94-17156, and the DGICYT (Spain) grant PB93-0820-C02-02.
[2] Dipartimento di Astronomia, Università di Bologna, CP 596, I-40100 Bologna, Italy; ritossa@astbo3.bo.astro.it.

[3] Departament de Física Aplicada, Universitat Politécnica de Catalunya, Jordi Girona Salgado s/n, Módulo B4—Campus Nord, 08034 Barcelona, Spain; garcia@etseccpb.upc.es.

[4] Departments of Astronomy and Physics, University of Illinois, 1002 West Green Street, Urbana, IL 61801; icko@sirius.astro.uiuc.edu.

white dwarf formed by our TPSAGB model is $\sim 1.26\ M_\odot$, the outer $0.06\ M_\odot$ of which is composed primarily of carbon and oxygen.

Subject headings: novae, cataclysmic variables — nuclear reactions, nucleosynthesis, abundances — stars: abundances — stars: AGB and post-AGB — stars: evolution — stars: interiors — stars: variables: long-period variables

1. INTRODUCTION

This paper is the second in a series of explorations of the behavior of stellar models which experience carbon burning under conditions of partial electron degeneracy. Paper I (García-Berro & Iben 1994) follows the evolution of a 10 $M_\odot$ model through the core carbon-burning phase prior to the onset of thermal pulses triggered by thermonuclear runaways in a helium-burning shell. The present paper repeats, with a larger nuclear-burning network and with the elimination of two crucial errors, the evolution described in Paper I and then follows the evolution of the model as carbon burning dies out and thermal pulses occur.

The major difference between results found here and in Paper I is that the mass of the ONe core is $\sim 1.2\ M_\odot$ rather than $\sim 1.3\ M_\odot$ as obtained in Paper I. Except near the surface of the core, the interior composition is similar to that found in Paper I, an important agreement being that the abundance by number of ^{23}Na is greater than that of ^{24}Mg over most of the interior. During the carbon-burning phase, radius and surface luminosity are almost exactly correlated. The reason for this is that the deep convective envelope is essentially "transparent" to the luminosity entering its base, and the relationship between surface luminosity and radius is set by the radiative atmosphere in which the dominant source of opacity is the H^- ion. The correlation obtained in the stellar model calculations can be approximated by employing a very simple analytical model of the stellar atmosphere at optical depths less than unity and an approximation to the H^- opacity.

The calculations are carried further than in Paper I to show that, as the second dredge-up episode continues, the radius expands from a minimum of $\sim 275\ R_\odot$ to $\sim 600\ R_\odot$ as some energy from the carbon-burning region leaks out to the surface. The carbon-burning luminosity continues to decrease, and radius expansion is temporarily reversed when the helium-burning luminosity also begins to decrease.

One of the primary motivations for constructing thermally pulsing "super"–asymptotic giant branch models (TPSAGB models = TPAGB models with ONe cores) is that no such models yet exist in the literature, even though 30 years have elapsed since the discovery of the thermal pulse phenomenon (Schwarzschild & Härm 1965; Weigert 1966). In several early studies, the thermal pulse instability has been suppressed in order to concentrate on the growth of a CO core to large masses (Arnett 1969; Uus 1970). Nomoto (1984, 1987) has constructed models with ONe cores, demonstrating that, following a second dredge-up episode, hydrogen is reignited, but he then suppresses the instability in the helium-burning shell in order to follow the growth of the ONe core up to the effective Chandrasekhar limit. In several other studies, the suppression mechanism is suspended at several different values of core mass in order to study one or two thermal pulses (Paczyński 1970; Sugimoto & Nomoto 1975; Iben 1977). The drawback of such studies is that there is no guarantee that the resultant flashes have characteristics which are close to those achieved after enough flashes have been followed to approach a local limit cycle.

A possible reason for the absence of TPSAGB models in the literature is that calculating the conversion of a CO core into an ONe core with traditional stellar evolution techniques is a very delicate and time-consuming task. Carbon burning is ignited off center, and structure variables vary almost discontinuously through the burning front. Timmes, Woosley, & Taam (1994) point out that "adequate resolution of the burning region would require zones finer than about 1 km." We resolve the front and find that zoning even finer than this is necessary to achieve convergence. During most of the carbon-burning phase, the "balanced-power" condition (carbon-burning luminosity = neutrino luminosity) which Timmes et al. (1994) adopt is not fulfilled, so there is no alternative but to follow the evolution by standard techniques. However, during the relatively short time when the front propagates inward and reaches the center, the varying velocity of the front agrees with velocities derived by Timmes et al. (1994) for appropriate densities, temperatures, and compositions.

In any case, one TPSAGB model now exists. We have followed the evolution of 30 thermal pulses, sufficient to establish that carbon which has been freshly made in a convective shell during a helium-shell flash is dredged up during pulse powerdown, that the temperatures in the convective shell become large enough for the ^{22}Ne(α, n)^{25}Mg reaction to be a potent neutron source for s-process nucleosynthesis (20–30 neutrons per ^{56}Fe seed), and to infer other limit-cycle behavior. The time between pulses is ~ 200 yr, close to the value of 180 yr given by the expression $\tau_{\rm interpulse} \sim 6 \times 10^5\ {\rm yr}\ (0.6\ M_\odot/M_{\rm core})^{10}$ (e.g., Iben 1991); the maximum and minimum helium-burning luminosities during a pulse cycle are $L_{\rm He}^{\rm max} \sim 2.7 \times 10^6\ L_\odot$ and $L_{\rm He}^{\rm min} \sim 100\ L_\odot$, respectively; and the maximum and minimum hydrogen-burning luminosities during a pulse cycle are $L_{\rm H}^{\rm max} \sim 6 \times 10^4\ L_\odot$ and $L_{\rm H}^{\rm min} \sim 100\ L_\odot$, respectively. The mean surface luminosity between pulses approaches $L_S = 6.4 \times 10^4\ L_\odot$ ($M_{\rm bol} = -7.25$).

A real (single star) counterpart of our model is expected to lose mass from the surface, eventually at a very high rate, and evolve into the central star of a planetary nebula. At a mass-loss rate of $\sim 10^{-4}\ M_\odot\ {\rm yr}^{-1}$ (which is typical of AGB stars supporting OH/IR winds) the TPSAGB phase will last $\sim 10^5$ yr, during which roughly 500 pulses occur. Taking dredge-up into account, the effective rate at which mass is added to the hydrogen-exhausted core is $\sim 10^{-4}\ M_\odot$ per pulse cycle, suggesting that the core mass of a real counterpart increases by $\sim 0.05\ M_\odot$ during the TPSAGB phase. We choose not to make the explicit calculations, but note that, in experiments with models of core mass small enough that such calculations are practical, the end result of the mass-loss episode is a hot white dwarf of mass essentially equal to that of the hydrogen-exhausted core, which, in our case, is $\sim 1.26\ M_\odot$. If the real counterpart of the remnant continues to lose mass at the maximum rate predicted by a radiative wind, both the hydrogen-rich and helium-rich

layers are removed by the time the remnant has evolved into a cool white dwarf (e.g., Iben & Tutukov 1996). Thus, the end result of the evolution of a single 10 $M_\odot$ star of Population I composition may be a 1.26 $M_\odot$ non-DA white dwarf with an ONe core of mass $\sim 1.20\ M_\odot$ and a CO layer of mass $\sim 0.06\ M_\odot$. Particle diffusion will result in a surface abundance dominated by carbon.

If the real counterpart is in a binary with a low mass secondary, and if it fills its Roche lobe after the main carbon-burning phase is completed but before thermal pulses begin, a common envelope forms, and mass loss from the system continues until the mass of the remaining hydrogen-rich layer is $\sim 10^{-5}\ M_\odot$, or approximately 10% of the mass through which the hydrogen-burning shell moves between pulses. The composition in the interior is expected to be essentially the same as that of the core of the primary at the beginning of the Roche lobe overflow episode. Below the hydrogen-rich layer is a layer of helium of mass $\sim 2 \times 10^{-4}\ M_\odot$, and below the helium layer is a CO layer of mass $\sim 0.015\ M_\odot$. In the outer 0.01 $M_\odot$ of this layer, there is essentially no Ne, either in the form of ^{20}Ne or in the form of ^{22}Ne. The dominant trace isotope in this Ne-free region is ^{25}Mg.

As the remnant evolves into a white dwarf, mass loss via a radiative wind removes both the hydrogen-rich layer and the helium-rich layer, leaving the Ne-free, Mg-enhanced layer exposed. When mass transfer from the low mass main-sequence secondary onto the white dwarf commences, nova outbursts triggered by hydrogen burning will at first be overabundant in Mg (as well as in C and O) and underabundant in Ne.

An estimate can be made of the fraction of novae produced by white dwarfs with ONe cores made by this scenario which will exhibit this abundance anomaly. At typical mass transfer rates of $\sim 10^{-9}$ to $10^{-8}\ M_\odot\ \mathrm{yr}^{-1}$, approximately $10^{-5}\ M_\odot$ of hydrogen-rich material must be transferred before a nova outburst occurs (e.g., Schwartzman, Kovetz, & Prialnik 1994). Assuming that the mixing between white dwarf matter and accreted matter results in a hydrogen profile extending a distance of $\sim 10^{-5}\ M_\odot$ into the white dwarf (e.g., Fujimoto & Iben 1992), and that approximately $2 \times 10^{-5}\ M_\odot$ is lost in the explosion, the Ne-free layer will be removed after ~ 1000 outbursts. If the initial mass of the main-sequence companion is $\sim 0.5\ M_\odot$, and if mass transfer at a high rate ceases once companion mass is reduced to $\sim 0.3\ M_\odot$, approximately 20,000 Ne-rich outbursts will occur at a frequency of roughly a few times 10^4 yr. Thus, perhaps one out of 20 novae produced by accreting white dwarfs with ONe cores will exhibit the abundance anomaly.

In § 2 we describe the evolution and composition of the constant mass model of mass 10 $M_\odot$ and metallicity $Z = 0.02$ during the carbon-burning phase, prior to the reactivation of hydrogen burning. In § 3 we describe the thermally pulsing phase, and in § 4 we provide a summary and discussion.

2. EVOLUTION AND COMPOSITION DURING THE CARBON-BURNING PHASE

Evolution up to the ignition of carbon is identical with that described in Paper I. Two errors which affected evolution during the carbon-burning phase have been found and corrected. The first error involves the location of the interface between the helium-exhausted core (where a carbon-burning code is used) and the rest of the model (where a hydrogen- and helium-burning network is used). The error caused this location to move back and forth in mass and affected abundances. The second error was a misplaced integer in the carbon-burning network which led to an incorrect calculation of nuclear transformations in convective regions. The corrected code gives results which are essentially the same as previously obtained with regard to the timescale and the global variations which take place during carbon-burning, but there are substantial differences in (1) the mass of the hydrogen-exhaused core after the second dredge-up episode and (2) the abundances of isotopes in the core after carbon-burning has been completed.

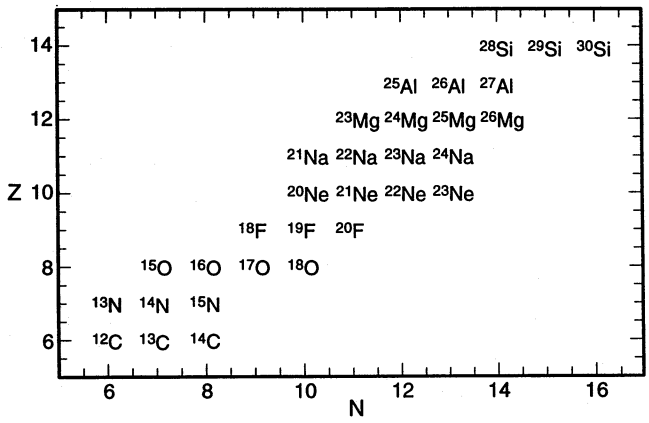

FIG. 1.—Carbon-burning reaction network. All reactions connecting the isotopes shown by n, p, α, $e^{\pm}$, and γ capture or decay are taken into account. The $^{12}C + {}^{12}C$ reactions are also, of course, taken into account.

Given the necessity of recomputing the carbon-burning phase, the original reaction network has been enlarged to include 17 additional isotopes. All reactions involving proton, neutron, alpha-particle, and gamma-ray captures and emissions, and all beta-decay reactions which cause transformations between the isotopes shown in Figure 1 have been taken into account, using the sources cited in Paper I for reaction cross sections.

The abundances by mass of the major isotopes in the hydrogen-exhausted core of mass $\sim 2.4\ M_\odot$ near the start of the carbon-burning phase (time $t = 7.1800943 \times 10^{14}$ s) are shown in Figure 2. Over that part of the core not shown in Figure 2, the abundance by number of ^{14}N is approximately equal to the sum of the abundances of ^{12}C, ^{14}N, and ^{16}O in the mix of abundances in the initial model (initial abundances by mass are $X_C:X_N:X_O = 0.00284:0.00093:0.00847$). An interesting feature of the abundance distribution in the CO core is that approximately one-third of the initial CNO elements has been converted into ^{25}Mg by the reaction ^{22}Ne(α, n)^{25}Mg, and the neutrons released in this reaction have contributed to the production of light s-process isotopes. This is consistent with the results of Iben & Tutukov (1985) for a 9.85 $M_\odot$ remnant of a case B mass-loss event. The number of neutrons released per iron seed is ~ 11, which compares with a release of ~ 2 neutrons per iron seed in a 9 $M_\odot$ model and ~ 16 neutrons per iron seed in a 15 $M_\odot$ model found by Lamb et al. (1977).

The evolution with time of several interior and global characteristics during the carbon-burning phase is shown in Figure 3. The duration of the phase is $\sim 2 \times 10^4$ yr, as found in Paper I and by Dominguez, Tornambè, & Isern (1993) in a study of a 10 $M_\odot$ star of metallicity $Z = 0.04$

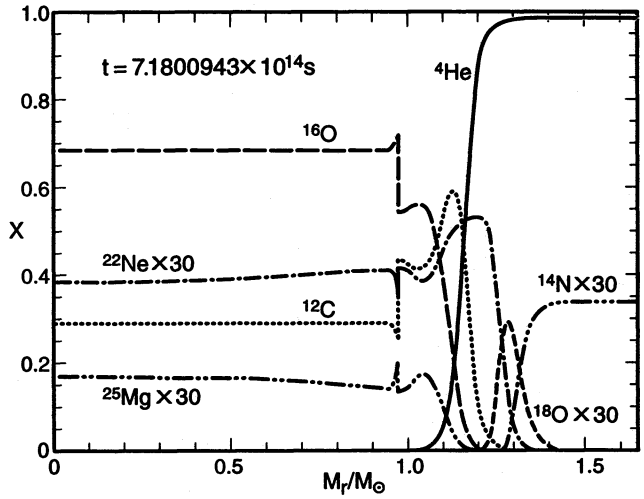

FIG. 2.—Abundances of major isotopes in the hydrogen-exhausted core of a 10 $M_\odot$ model of Population I initial composition at the beginning of carbon burning (time $t = 7.1800943 \times 10^{14}$ s).

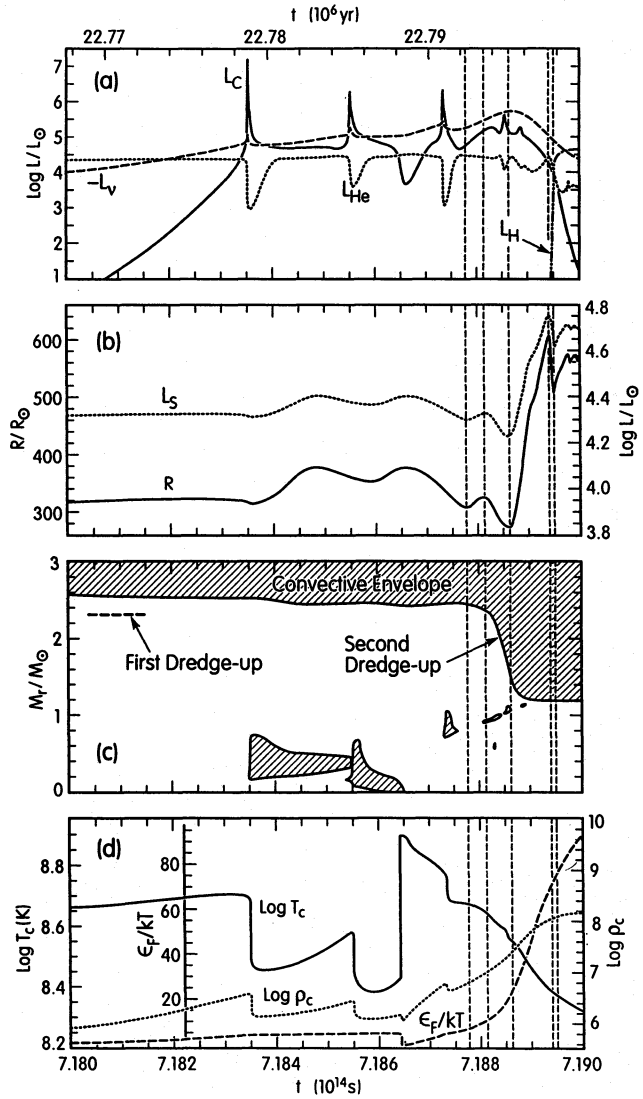

FIG. 3.—Global and internal characteristics of the 10 $M_\odot$ model during the carbon-burning phase. (*a*) Carbon-burning luminosity L_C, helium-burning luminosity L_{He}, hydrogen-burning luminosity L_H, and neutrino loss rate $-L_\nu$. (*b*) Stellar radius R and luminosity L_S. (*c*) Location of the boundaries of convective layers. (*d*) Central temperature T_c, density ρ_c, and the electron Fermi energy ϵ_F divided by kT.

which has been stripped of its hydrogen-rich envelope in a simulated common envelope event that is imposed at the beginning of the core helium-burning phase. Several correlations among the variables in Figure 3 are worth emphasizing.

The correlation between radius and surface luminosity (Fig. 3*b*) is striking and easy to understand qualitatively. The convective envelope is effectively "transparent" to the flow of energy through it, in the sense that the luminosity at its outer edge is essentially the same as at its inner edge. Thus, the only connection between radius and luminosity is established in the very outer (optical depth $\leq \frac{2}{3}$) radiative atmosphere from which photons flow into free space. In very rough approximation, state variables (pressure P, density ρ, and temperature T) and opacity κ at the base of this atmosphere are related by

$$P \sim \frac{k}{\mu M_H} \rho T \sim \frac{2}{3} \frac{GM}{R^2} \frac{1}{\kappa},$$

where M and R are, respectively, the mass and radius of the model, G is the gravitational constant, k is Boltzmann's constant, μ is the mean molecular weight, and M_H is the mass of the hydrogen atom. Further, the temperature T at the base of the atmosphere is related to the model luminosity L and radius by

$$T^4 \propto \frac{L}{R^2}.$$

Assuming that the dominant opacity source is the negative hydrogen atom, so that (see Hansen & Kawaler 1994)

$$\kappa \propto \rho^{1/2} T^9,$$

and setting $\rho^{3/2} \propto T^m$, where $m > 0$, one has

$$\left(2 - \frac{8}{10 + m}\right) \log R \sim \log L + \text{constant},$$

showing that stellar radius and luminosity vary in step with one another. If, for example, $\rho \propto T^3$, then $m = 4.5$ and $d \log L/d \log R \sim 1.45$, which compares favorably with $d \log L/d \log R \sim 1.5$ found in the model calculations.

Other correlations are apparent in Figure 3. At the start of each carbon-burning flash (Fig. 3*a*), an interior convective zone (Fig. 3*c*) develops in response to the rapid injection of nuclear energy, and the zone persists during a following period of quiescent carbon-burning. In the first two flashes, the injected energy causes expansion of overlying layers, leading to a reduction in the helium-burning luminosity. The reduction in the pressure on the matter interior to the carbon-burning shell causes this matter to expand and cool. During the quiescent carbon-burning phase following the second flash, the base of the associated convective shell reaches the center, whereupon the degeneracy there is removed (see ϵ_F/kT in Fig. 3*d*).

It is of interest to compare the velocity of the burning front at the base of the convective shell as it approaches the center with the velocity given by a theory of flame fronts developed by Timmes & Woosley (1992) and Timmes et al. (1994). Under the assumption that the nuclear energy produced in the front equals the total rate of neutrino losses in an associated convective shell, these authors show that the velocity of the front can be estimated from the local state and composition variables. The balanced-power assumption is approximately fulfilled (to within a factor of 2 in the

time period $t = (7.1855–7.1864) \times 10^{14}$ s) during the final approach of the base of the convective shell toward the center (see Figs. 3*a* and 3*c*). Therefore, the Timmes et al. (1994) velocity estimates should be similar to the velocities which we obtain, and this is indeed the case. For example, at a time $t \sim 7.186 \times 10^{14}$ s, when the front in our calculation is at a distance $r = 2500$ km ($0.036\ M_\odot$) from the center, its spatial velocity is $v \sim 3 \times 10^{-3}$ cm s^{-1}; this compares with the flame velocity $v \sim 2.8 \times 10^{-3}$ cm s^{-1} obtained by interpolation in the tables of Timmes et al. (1994) for the same conditions [$\rho \sim 6.5 \times 10^5$ g cm^{-3}, $T \sim 0.76 \times 10^9$ K, $X(^{12}C) \sim 0.3$, and $X(^{16}O) \sim 0.7$]. In our calculations, the zoning in the front is $\sim$0.2 km, well within the $\sim$1 km minimum stipulated by Timmes et al. (1994) for resolution of the front. In Paper III (García-Berro, Ritossa, & Iben 1996), we explore further the comparison with the Timmes et al. (1994) estimates of front velocity in the context of a 9 $M_\odot$ model which has a more degenerate core within which the balanced-power approximation is fulfilled over a larger fraction of the carbon-burning phase than in the 10 $M_\odot$ model.

The third carbon shell flash evokes a response similar to that of the first two, but the response at the center is less pronounced owing to the larger mass separating the carbon-burning zone and the center. The abrupt drop in the central temperature is superimposed on a steady decline which begins after the burning front has reached the center; the steady decline is due to neutrino losses.

A mild flash activity accompanies the final rise and fall in the carbon-burning luminosity L_C. During this last carbon-burning phase, the burning front approaches the helium-burning shell, and a nonnegligible fraction of L_C finds its way out to the radiative layer separating the helium-burning shell and the base of the convective envelope (Fig. 24 in Paper I). This is in contrast to prior flash episodes when most of the carbon-burning luminosity is lost to neutrinos or is absorbed between the carbon-burning shell and the helium-burning shell (Fig. 13 in Paper I). The energy absorbed in the radiative zone between the helium-burning shell and the base of the convective envelope causes expansion, cooling, and a consequent inward penetration in mass of the base of the convective envelope (from $\sim$2.5 $M_\odot$ to $\sim$1.2 $M_\odot$). This phase is called the "second dredge-up" phase (e.g., Becker & Iben 1979).

The development of the dredge-up episode is best described with the help of Figure 4, where luminosity and velocity in the model star are shown at four times: (*a*) near the beginning of the dredge-up phase as radius is shrinking ($t = 7.188255 \times 10^{14}$ s), (*b*) when the radius reaches a relative minimum ($t = 7.188540 \times 10^{14}$ s), and (*c*) and (*d*) during the overall envelope expansion phase ($t = 7.188936 \times 10^{14}$ s and $t = 7.189128 \times 10^{14}$ s, respectively). To avoid the impression of a discontinuity, the velocity distribution is shown in Figure 4 (*bottom panel*) at two additional times (*b*′ and *b*″) between those at (*b*) and (*c*).

Thanks to leakage from the carbon-burning region, the luminosity flowing into the base of the helium-burning shell, when added to that produced within the helium-burning shell, increases with time, even during that portion of the dredge-up episode when both the carbon-burning luminosity and the helium-burning luminosity decrease. During the first part of the dredge-up episode, the absorption in the radiative zone between the helium-burning shell and the base of the convective envelope increases more

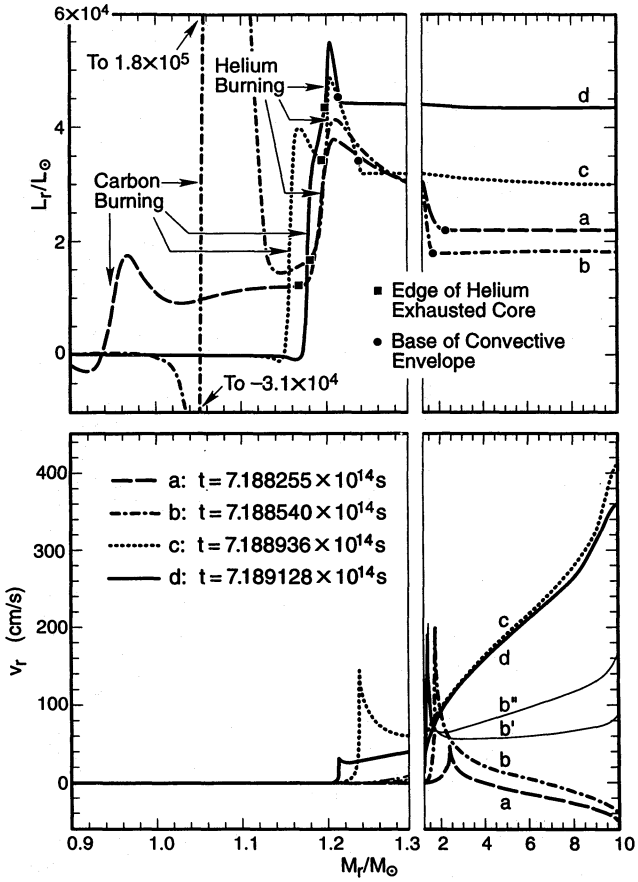

FIG. 4.—Luminosity (*upper panel*) and velocity (*lower panel*) as a function of mass at four different times (*a–d*) during the second dredge-up episode. The location of the base of the convective envelope (CE base) and the location of the helium-burning shell are indicated on each curve. The location of the base of the convective envelope at the end of the first dredge-up phase is shown by the dashed-line segment. Velocity profiles for two times intermediate between those for *b* and *c* are also shown: the times are (*b*′) 7.188690×10^{14} s and (*b*″) 7.188720×10^{14} s.

rapidly than the luminosity passing through the helium-burning shell increases; hence, the luminosity at the base of the convective envelope decreases, and the outer parts of the envelope contract in order to satisfy the requirements of the radiative atmosphere. Superimposed on this response of surface layers to a decreasing luminosity is a reduction in the number of particles per gram supplying pressure in the envelope (as helium is dredged up), but this reduction contributes insignificantly to the tendency for the radius to shrink. As the base of the convective envelope approaches the helium-burning shell, the radiative layer becomes less massive and absorbs energy more slowly than (thanks to leakage from the carbon-burning region) the luminosity through the helium-burning shell increases; the luminosity reaching the base of the convective envelope increases with time, and the outer parts of the envelope therefore expand.

The variations in radius are interesting from the perspective of binary star evolution. During quiescent carbon-burning following the first carbon-shell flash (L_C in Fig. 3*a*), the radius of the model increases from $\sim$325 $R_\odot$ to $\sim$375 $R_\odot$ (Fig. 3*b*). During the completion of the second dredge-up episode, the radius increases to $\sim$600 $R_\odot$, decreases temporarily as L_{He} decreases, and then increases again as hydrogen begins to burn strongly at the base of the H-He discontinuity. In a close binary with a 10 $M_\odot$ primary

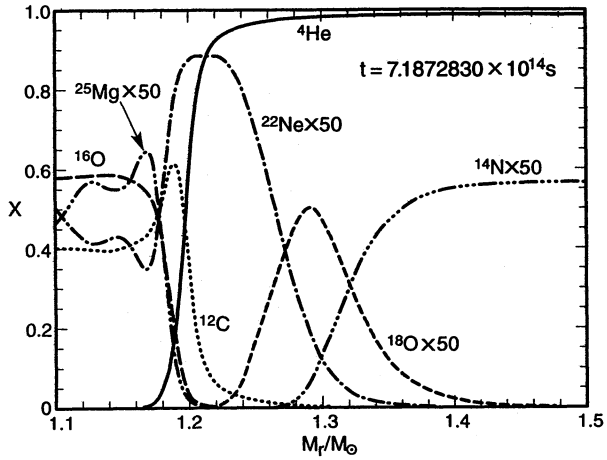

FIG. 5.—Abundances by mass of several isotopes just prior to the second dredge-up episode ($t = 7.1872830 \times 10^{14}$ s).

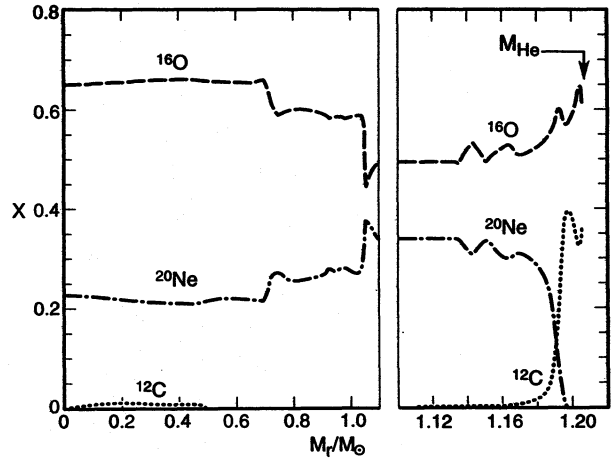

FIG. 7.—Abundances by mass of the major isotopes in the helium-exhausted interior at the end of the carbon-burning phase ($t = 7.1895212 \times 10^{14}$ s).

which escapes Roche lobe filling prior to the ignition of carbon, it is more likely that, because of a larger phase space, Roche lobe filling and mass transfer will begin during the radius-increasing part of the second dredge-up episode than that it will begin early on in the carbon-burning phase. Assuming that the probability of Roche lobe filling is proportional to $\Delta \log R$ (Iben & Tutukov 1984), the ratio of probabilities is log (600/375)/log (375/325) ~ 3.3.

Abundances in the neighborhood of the carbon-helium (C-He) interface just prior to the second dredge-up episode are shown in Figure 5 ($t = 7.1872830 \times 10^{14}$ s). The C-He interface is near 1.2 $M_\odot$ rather than near 1.3 $M_\odot$ as in Paper I (Fig. 26). Abundances in the neighborhood of the C-He interface when the second dredge-up episode is completed are shown in Figure 6 ($t = 7.1894812 \times 10^{14}$ s). The mass of the hydrogen-exhausted core is ~1.207 $M_\odot$ rather than ~1.316 $M_\odot$ as in Paper I (Fig. 27). It is interesting that dredge-up continues until the base of the convective envelope extends into a region where fresh carbon has been produced. At the end of the dredge-up episode, surface abundances by mass are $X(^1\text{H}) = 0.590$, $X(^3\text{He}) = 1.03 \times 10^{-5}$, $X(^4\text{He}) = 0.397$, $X(^{12}\text{C}) = 0.00187$, $X(^{14}\text{N}) = 0.00394$, $X(^{16}\text{O}) = 0.00665$, $X(^{18}\text{O}) = 8.62 \times 10^{-5}$, $X(^{22}\text{Ne}) = 1.31 \times 10^{-4}$, and $X(^{25}\text{Mg}) = 1.11 \times 10^{-7}$.

Abundances in the interior after carbon-burning has been completed are shown in Figures 7–9. Several features of these abundance distributions deserve comment: (1) The abundance profiles of ^{16}O, ^{20}Ne, and ^{24}Mg in the interior are in reasonable agreement with those obtained by Dominguez et al. (1993). (2) Over most of the interior, ^{23}Na is more abundant than ^{24}Mg, as found by Lamb, Iben, & Howard (1975) and in Paper I. (3) The ^{12}C abundance profile over the inner 0.5 $M_\odot$ is similar to the profile found by Nomoto (1984) but does not exhibit the large spike near the center found by Dominguez et al. (1993). (4) There is a layer of mass ~0.015 $M_\odot$ between the ONe core and the overlying helium-rich layer which consists primarily of carbon and oxygen. (5) Over the outer 0.01 $M_\odot$ of the CO layer, the abundances of all neon isotopes are much smaller than solar.

Points 2 and 3 have ramifications for the behavior of an accreting white dwarf which reaches the effective Chandrasekhar mass of ~1.37–1.39 $M_\odot$ (Boozer, Joss, & Salpeter 1973; Nomoto 1984, 1987), and points 4 and 5 have rami-

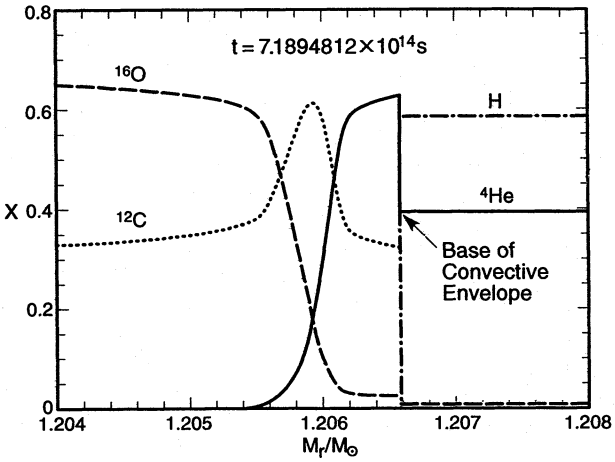

FIG. 6.—Abundances by mass of the major isotopes near the base of the convective envelope (at ~1.2066 $M_\odot$) at the end of the second dredge-up phase ($t = 7.1894812 \times 10^{14}$ s).

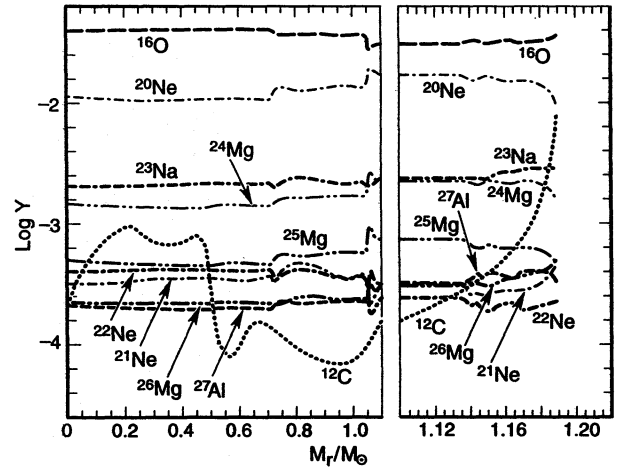

FIG. 8.—Abundances by number of several isotopes in the helium-exhausted interior at the end of the carbon-burning phase ($t = 7.1895212 \times 10^{14}$ s).

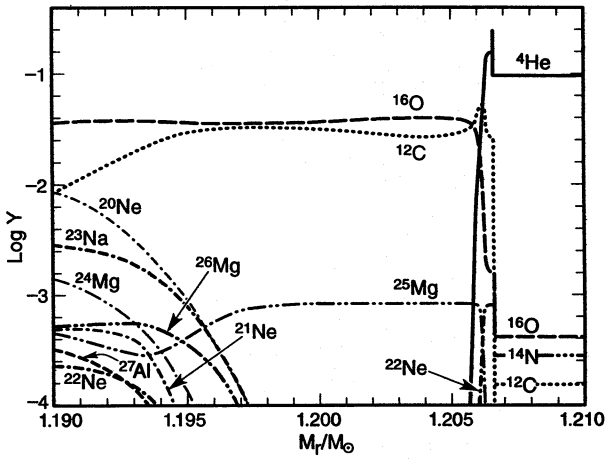

FIG. 9.—Abundances by number of several isotopes in the transition zone between the carbon-burned interior and the helium buffer layer at the end of the carbon-burning phase ($t = 7.1895212 \times 10^{14}$ s).

fications for the formation of Ne-rich novae. The relevance to stars in close binaries is due to the fact that the white dwarf in a cataclysmic variable (CV) has initial interior abundance characteristics very close to those in the core of a single star of the same mass as the white dwarf progenitor when it first reaches the TPAGB phase (e.g., Iben & Tutukov 1985, 1996).

As found in studies of electron-capture–induced core collapse (Finzi & Wolf 1967; Rakavy, Shaviv, & Zinamon 1967), electron captures on ^{24}Mg and ^{20}Ne cause contraction and heating to the extent that explosive oxygen-neon burning is initiated (Miyaji et al. 1980; Miyaji & Nomoto 1987). The subsequent competition between the tendency to collapse (due to electron capture on the products of fusion reactions) and the tendency to expand (due to the explosive nature of nuclear burning) is strong, and many subtle effects can affect whether the final outcome is collapse to a neutron star or disruption of the entire star (e.g., Canal, Isern, & Labay 1992; Hashimoto, Iwamoto, & Nomoto 1993; Gutiérrez et al. 1996). It is therefore important to include the appropriate abundances of both ^{23}Na and ^{24}Mg in collapse-explosion studies (see Paper I).

Studies of the nucleosynthesis during carbon-burning show that the ratio of ^{23}Na to ^{24}Mg depends on the extent to which carbon-burning has progressed and on the temperature and density at which carbon-burning takes place (e.g., Arnett & Truran 1969; Arnett 1973). Under conditions of constant (high) temperature and density, as carbon is depleted, the ratio of ^{24}Mg to ^{23}Na increases, and the final ratio is smaller, the lower the temperature. Under conditions in the model star discussed here, maximum temperatures during carbon burning are typically a modest ~ 0.7–0.8×10^9 K, and, in convective shells, the typical temperature sampled is even smaller than this. An explicit example of the flow of reactions is shown in Figure 10, which gives the major reaction channels in the first convective shell at a time $t = 7.1835122 \times 10^{14}$ s when the ^{12}C abundance is 0.0250 by number and the abundances by number of ^{23}Na and ^{24}Mg are, respectively, 5.53×10^{-4} and 8.99×10^{-5}. The ^{23}Na is formed primarily by the ^{12}C(^{12}C, p)^{23}Na reaction and is destroyed by the ^{23}Na(p, α)^{20}Ne and ^{23}Na(n, γ)^{24}Na reactions. The major source of ^{24}Mg is the beta decay of ^{24}Na, with the contribution of the ^{20}Ne(α, γ)^{24}Mg reaction being typically an order of magnitude smaller. Neutrons to convert ^{23}Na into ^{24}Na are produced primarily by (α, n) reactions on ^{13}C, which is itself produced by the ^{12}C(p, γ)^{13}N(e^+, ν)^{13}C and ^{12}C(n, γ)^{13}C reactions. An example of how the abundances of ^{23}Na and ^{24}Mg vary with the abundance of ^{12}C is shown in Figure 11. The mass point at which abundances are given is 0.4 $M_\odot$, and the time interval covers the duration of the first and second convective shells.

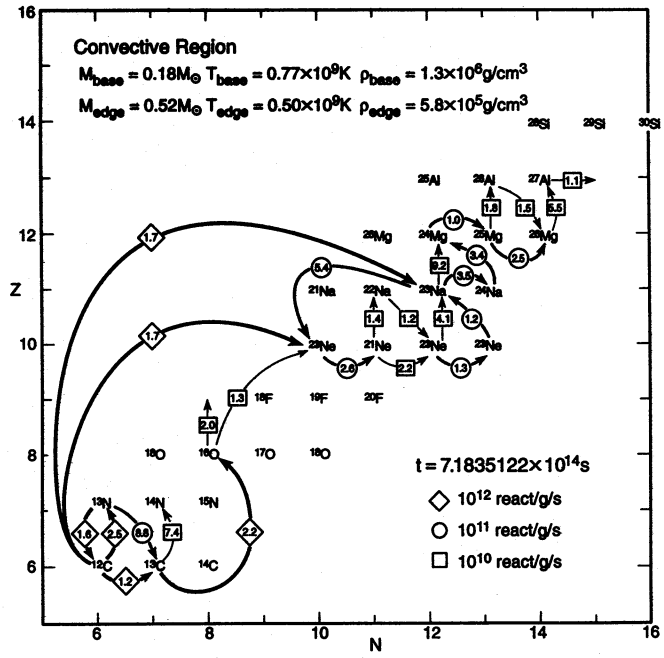

FIG. 10.—Major reaction channels in the convective shell at time $t = 7.1835122 \times 10^{14}$ s.

Dominguez et al. (1993) find that, after carbon-burning is completed in models of metallicity $Z = 0.04$ and of initial masses 10 and 10.5 $M_\odot$ which are stripped of their hydrogen-rich envelopes, the abundance by mass of ^{12}C in a central spike is quite large [$X(^{12}\text{C}) \sim 0.23$]. If an observational counterpart accretes enough mass from a companion to achieve the effective Chandrasekhar limit, collapse due to electron captures on ^{24}Mg will cause the temperature to increase until carbon is reignited. Carbon-burning (at an initial carbon abundance by mass of 0.23 and an energy release of $\sim 7 \times 10^{17}$ ergs g^{-1}) causes the tem-

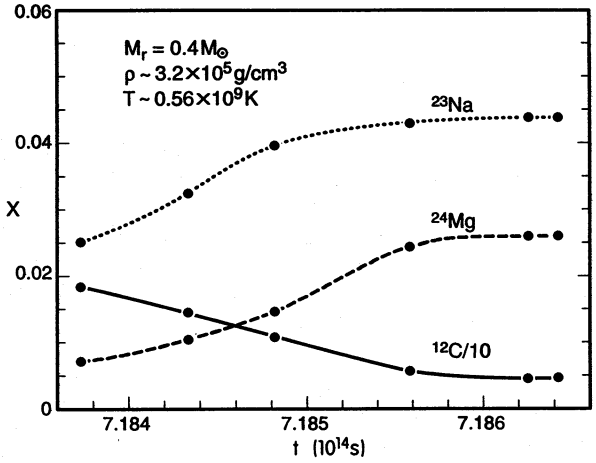

FIG. 11.—Abundances by mass vs. time of ^{12}C, ^{24}Mg, and ^{23}Na at mass point 0.4 $M_\odot$. The temperature is $\sim 0.5 \times 10^9$ K, and the mean density is $\sim 3 \times 10^5$ g cm^{-3}.

perature to increase sufficiently for oxygen to ignite. The resulting explosion, beginning at lower densities than would have been the case in the absence of a central spike of ^{12}C, is expected to disrupt the star.

However, with ^{12}C at the abundance found in the mass-conservative calculations of Nomoto (1984) and here [$X(^{12}C) \sim 0.01$; see Figs. 7 and 8], the local temperature can be increased to only $\sim 10^9$ K; this is not enough to initiate oxygen burning. Clearly, it is important to investigate further the behavior of nonconservative models as a function of the evolutionary phase at which Roche lobe overflow first occurs. The properties of the young binary radio pulsar PSR 1718−19 in the globular cluster NGC 6342 (Lyne et al. 1993) suggest that the pulsar has been made by the collapse of an ONe white dwarf which has accreted from a low-mass companion (Wijers & Paczyński 1993). This implies that, in some instances at least, the carbon abundance in an ONe remnant white dwarf in a close binary is everywhere small [say, $X(^{12}C) \leq 0.01$]. This does not mean that the Dominguez et al. (1993) carbon spike is in error (as these authors suggest might be the case), since such a spike is Rayleigh-Taylor unstable and might be expected to be spread out over a much larger volume (Gutiérrez 1996).

Figures 7 and 9 show that, between the ONe core and the ^4He-^{14}N layer, there is a layer of mass $\sim 0.015\ M_\odot$ in which carbon and oxygen are the dominant elements and in the outer two-thirds of which there is essentially no ^{20}Ne or ^{22}Ne. In a close binary in which the primary fills its Roche lobe in a case C (and possibly also in a case B) event, the hydrogen-rich and helium-rich layers will probably be lost by a radiative wind following a common envelope event (Iben & Tutukov 1996), but the remnant white dwarf will retain the Ne-free layer, and, when mass transfer from the secondary to the white dwarf takes place, this Ne-free CO layer must be surmounted (see, e.g., Iben, Fujimoto, & MacDonald 1992) before the mixing of white dwarf matter with hydrogen-rich accreted matter leads to an excess of neon (whether ^{20}Ne or ^{22}Ne!) in the nova ejecta. On the other hand, the CO layer contains a large overabundance of ^{25}Mg (Fig. 8), and this might permit a distinction to be made between a nova in which the white dwarf has an ONe core and one in which the white dwarf has a CO core. In the latter case, in the CO zone below the helium buffer layer, the dominant isotope apart from ^{16}O and ^{12}C is ^{22}Ne (see Fig. 2).

3. REACTIVATION OF HYDROGEN BURNING, THE DEMISE OF CARBON BURNING, AND THERMAL PULSES

By the end of the second dredge-up episode, the center of the helium-burning shell is only $\sim 6 \times 10^{-4}\ M_\odot$ away from the base of the hydrogen-rich envelope, and, as helium-burning continues, the temperature at the H-He discontinuity increases to the extent that hydrogen-burning recommences. The suddenness with which hydrogen-burning is reactivated is shown in Figure 12*a* (curve labeled L_H).

It is evident that carbon burning becomes increasingly less important and eventually ceases to play a role in the evolution of the model, as demonstrated by Nomoto (1984). The decline in L_C (Fig. 12*a*) is due to the fact that, when carbon is exhausted over a sufficient fraction of the helium-exhausted core, the core contracts rapidly (see Fig. 3*d*), and

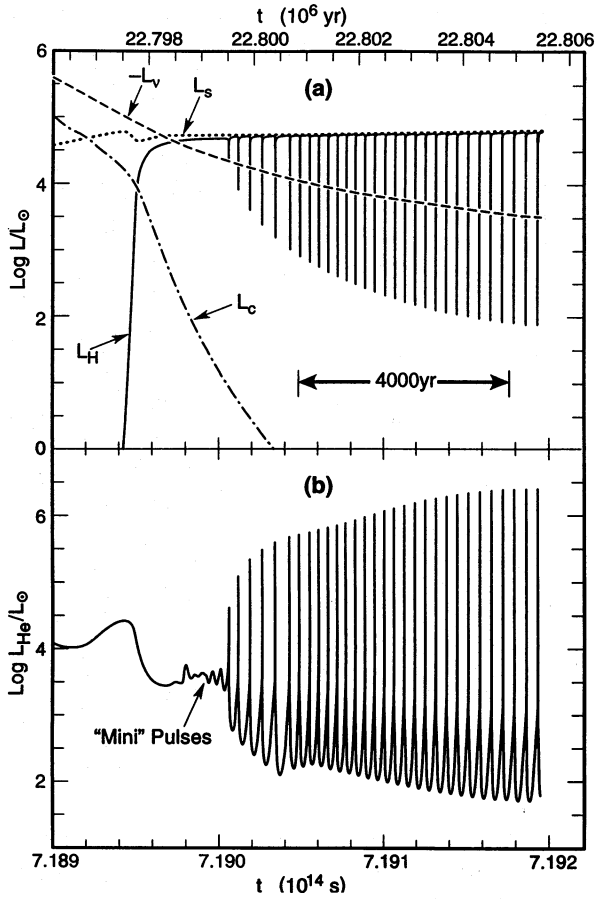

FIG. 12.—Reactivation of hydrogen-burning, demise of carbon-burning, and the onset of helium-shell flashes. (*a*) Time dependences of L_H (the hydrogen-burning luminosity), L_C (the carbon-burning luminosity), L_S (the surface luminosity) and $-L_\nu$ (the neutrino loss rate). (*b*) Helium-burning luminosity L_{He}.

the interior density structure approaches asymptotically that of a white dwarf of mass equal to the mass of the helium-exhausted core. The electron degeneracy in the interior is so high that the core can now contract only at a rate determined by the rate at which the mass of the helium-exhausted core increases (i.e., determined by the rate of helium burning). The temperatures in the carbon-rich layers are controlled by a balance between neutrino losses and the rate at which gravitational potential energy is released by the contracting layer of ash produced by the helium-burning shell. Ash is not produced rapidly enough for carbon to burn in steady state, so the temperatures in the carbon-rich layers drop until carbon burning is essentially completely extinguished. The temperature profiles in Figure 13 illustrate the cooling process. Eventually, the peak temperature will approach a steady state value of $\sim 150 \times 10^6$ K (see Fig. 9 in Iben 1982).

Uus (1970) shows by means of a linear analysis that the helium-burning shell above a massive degenerate core is thermally unstable, and Paczyński (1970), Sugimoto & Nomoto (1975), and Iben (1977) demonstrate this explicitly in models in which the instability is suppressed during the growth of the core to larger masses. If one views the physics of the situation to be that of a white dwarf accreting helium from the hydrogen-burning shell, the basic reason for the instability is that helium can burn as rapidly as it is accreted only for an accretion rate which is an order of magnitude

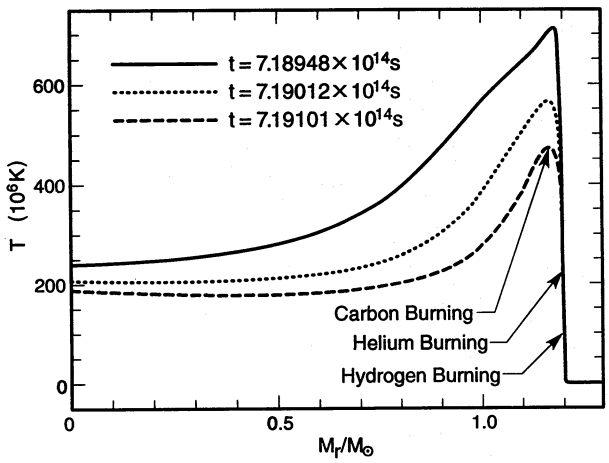

FIG. 13.—Temperature profiles in the helium-exhausted core at several times as $L_C \rightarrow 0$ permanently. The peak carbon-burning rate occurs at the temperature maximum.

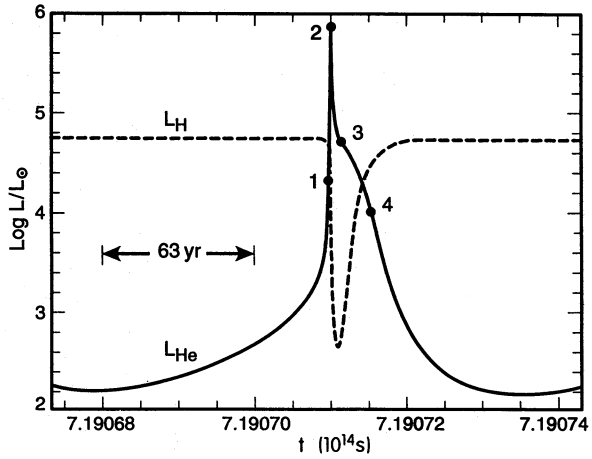

FIG. 14.—Nuclear-burning luminosities at the beginning of, during, and after the 11th helium-shell flash. Characteristics of the model at labeled points are shown in Figs. 15–19.

larger than the rate at which quiescent hydrogen-burning processes matter (Iben & Tutukov 1989, 1995).

The onset and growth of helium shell flashes and the effects of these flashes are described in Figures 12*b* and 12*a*, respectively. During the first few flashes (labeled "mini" pulses [Becker & Iben 1980] in Fig. 12*b*), the flux of helium-burning luminosity is not sufficient to create a convective shell. Even when fully developed, with convective shells forming, the flashes (Fig. 12*b*) are relatively mild and build up slowly to a peak value of $L_{He}^{max} \sim 2.7 \times 10^6\ L_\odot$ after 30 pulses. The time between flashes approaches ~200 yr.

The time dependences of the nuclear-burning luminosities L_{He} and L_H during the eleventh helium shell flash are shown in Figure 14. Composition, structure, and dynamical characteristics at the four stages labeled numerically in Figure 14 are given in Figures 15–19. The more traditionally described characteristics (energy generation rates, luminosity, and composition) are shown in the left-hand panels (*a* and *b*) of Figures 15–18, and the equally interesting dynamical characteristics (velocity, rates of temperature, and density changes) are shown in the right-hand panels (*c* and *d*). The radius at two mass points is given in panel (*c*), and the temperature is given in panel (*d*). Density profiles are given in Figure 19 for the models described in Figures 15–18.

At the stage described in Figure 15 (point 1 in Fig. 14, $t = 7.1907094 \times 10^{14}$ s, $L_{He} = 2.08 \times 10^4\ L_\odot$), energy production by helium-burning has not yet had a significant influence on hydrogen-burning characteristics (ϵ_n and L_r in Fig. 15*a*), but expansion in the helium-burning layers ($d \log \rho/dt$ in Fig. 15*c*) brought about by heating due to the injection of nuclear energy ($d \log T/dt$ in Fig. 15*d*) is causing

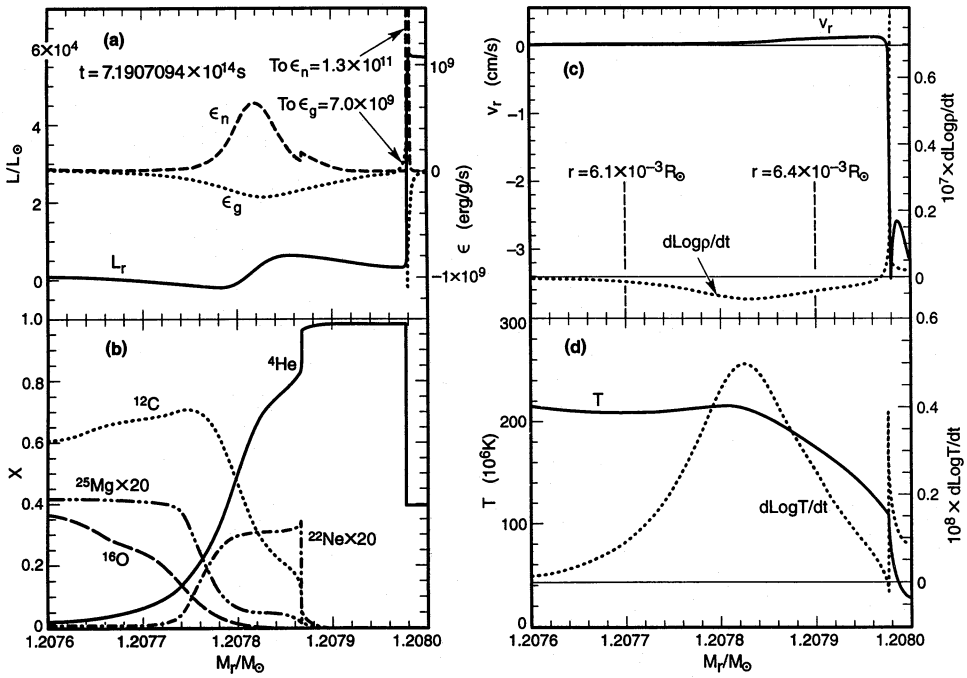

FIG. 15.—Composition and structure characteristics in the nuclear active region just before the 11th helium-shell flash ($t = 7.1907094 \times 10^{14}$ s, $L_{He} = 2.08 \times 10^4\ L_\odot$, point 1 in Fig. 14). Variables are (*a*) luminosity L_r, ϵ_{nuc}, ϵ_{grav}; (*b*) abundances by mass $X(^4\text{He})$, $X(^{12}\text{C})$, $X(^{16}\text{O})$, $X(^{22}\text{Ne})$, and $X(^{25}\text{Mg})$; (*c*) radial velocity v_r, density ρ, and $d \log \rho/dt$; and (*d*) temperature T and $d \log T/dt$.

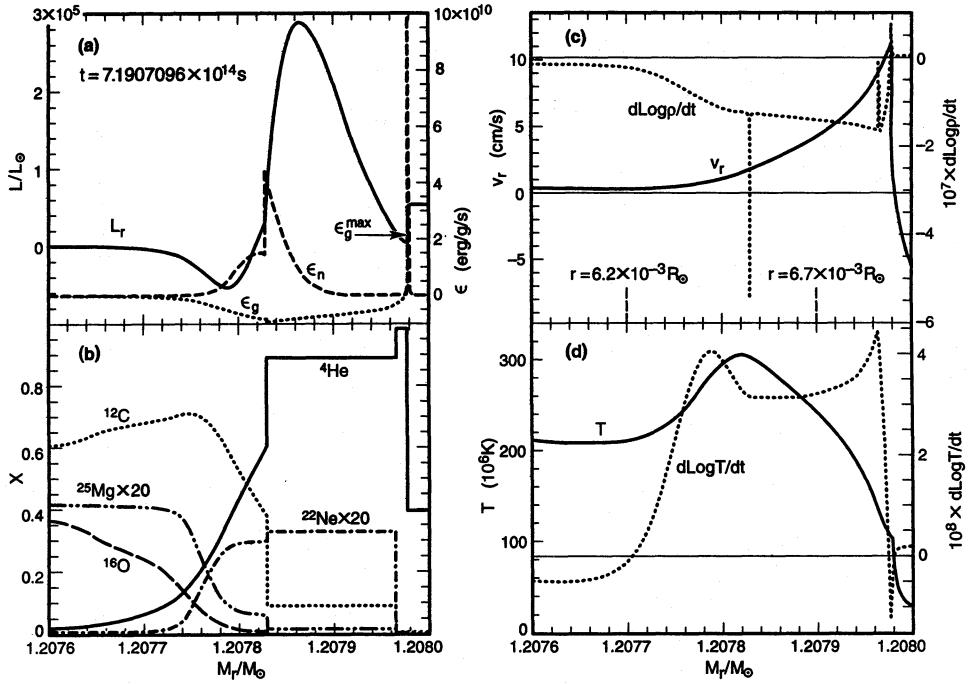

FIG. 16.—Composition and structure characteristics in the nuclear active region just before the peak of the 11th helium-shell flash ($t = 7.1907096 \times 10^{14}$ s, $L_{He} = 7.50 \times 10^5\ L_\odot$, point 2 in Fig. 14). Variables have the same meaning as in Fig. 15.

matter all the way from helium-burning layers to the base of the hydrogen-burning shell to move outward. In the hydrogen-burning region, matter is still moving inward ($v_r < 0$), being compressed ($d \log \rho/dt > 0$), and heated ($d \log T/dt > 0$). The temperature inversion that is a characconversion of nuclear energy into heat is already evident at this early stage of the thermal pulse (see Fig. 15*d* at $M_r/M_\odot \gtrsim 1.20781$).

At the stage described in Figure 16 (point 2 in Fig. 14, $t = 7.1907096 \times 10^{14}$ s, $L_{He} = 7.50 \times 10^5\ L_\odot$), the shell flash is well underway, with fully two-thirds of the nuclear energy produced by helium burning (Fig. 16*a*) used up in heating (Fig. 16*d*) and expanding (Fig. 16*c*) matter between the helium-burning region and the hydrogen-burning shell. Over most of the expanding region, matter is being heated, but in the neighborhood of the hydrogen-burning shell, matter is actually cooling (Fig. 16*d*), and this is responsible for the decline in L_H. The transition between heating and cooling takes place in the radiative region between the outer edge of the convective shell sustained by helium-burning

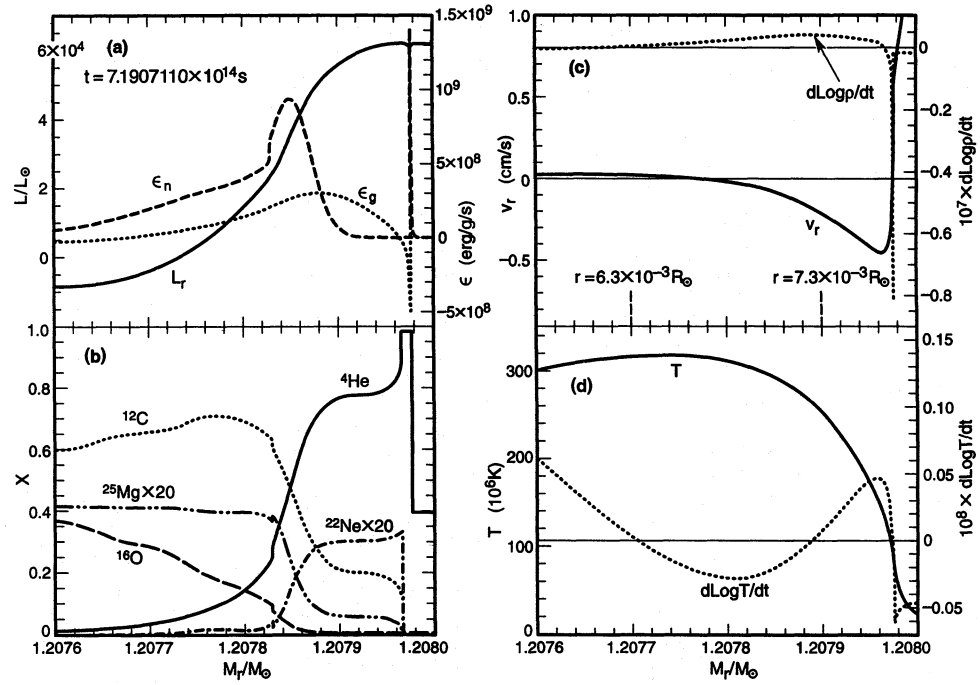

FIG. 17.—Composition and structure characteristics in the nuclear active region when L_H is at a minimum following the 11th helium-flash ($t = 7.1907110 \times 10^{14}$ s, $L_{He} = 5.08 \times 10^4\ L_\odot$, point 3 in Fig. 14). Variables have the same meaning as in Fig. 15.

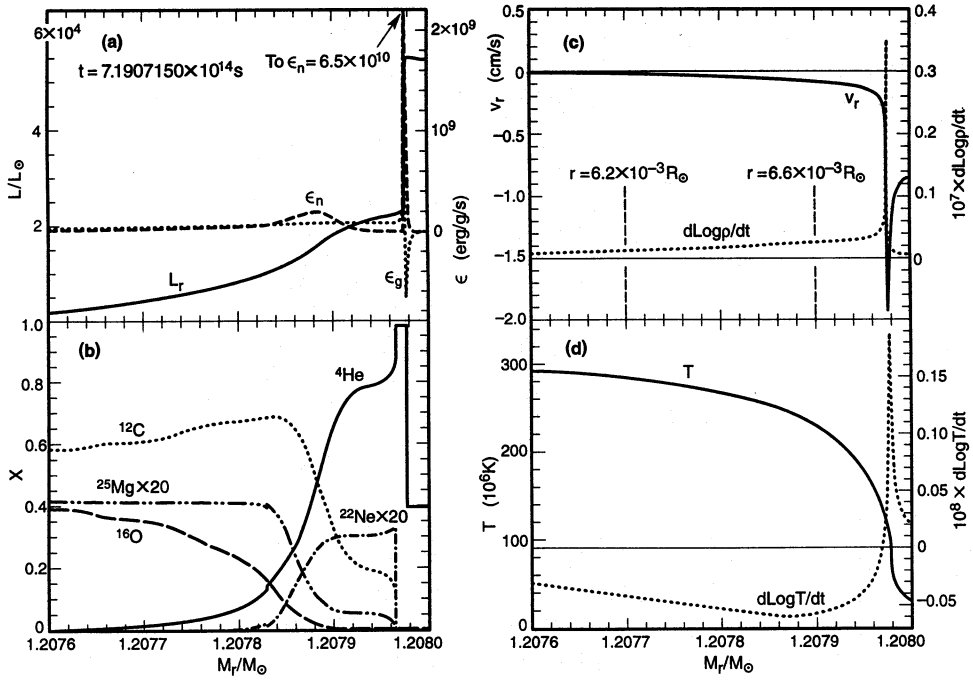

FIG. 18.—Composition and structure characteristics in the nuclear active region when $L_H \sim L_{He}$ following the 11th helium-shell flash ($t = 7.1907150 \times 10^{14}$ s, $L_{He} = 10^4\ L_\odot$, point 4 in Fig. 14). Variables have the same meaning as in Fig. 15.

(the convective zone is coincident with the flat portion of the ^{4}He and ^{12}C profiles centered at $M_r/M_\odot \sim 1.2079$ in Fig. 16*b*) and the hydrogen-burning shell. The beginning of a cooling zone near the base of the hydrogen-burning shell is already evident in Figure 15*d*.

At the stage described in Figure 17 (point 3 in Fig. 14, $t = 7.1907110 \times 10^{14}$ s, $L_{He} = 5.19 \times 10^4\ L_\odot$), the hydrogen-burning luminosity is at a relative minimum of $L_H \sim 600\ L_\odot$. Matter in the neighborhood of the hydrogen-burning shell is still cooling, expanding, and moving outward, but matter between the outer edge of the helium-burning region and just below the hydrogen-burning shell is contracting and heating. Matter in the helium-burning region is contracting, cooling, and moving inward.

At the stage described in Figure 18 (point 4 in Fig. 14, $t = 7.1907150 \times 10^{14}$ s, $L_{He} = 9.99 \times 10^3\ L_\odot$), the hydrogen-burning shell has almost recovered its preflash strength. All of the matter containing helium is moving inward, contracting, and cooling.

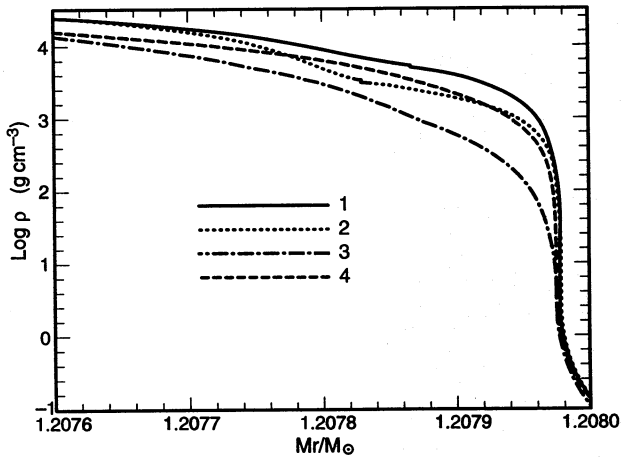

FIG. 19.—Density profiles for the models described in Figs. 15–18.

The variations in the composition profiles for ^{22}Ne and ^{25}Mg during the helium-burning phase (panels *b* in Figs. 15–18) are interesting from the point of view of neutron-capture nucleosynthesis. During the course of the 11th pulse, approximately 13% of the ^{22}Ne that is formed by reactions experienced by ^{14}N and its progeny in the convective shell is converted into ^{25}Mg by the ^{22}Ne(α, n)^{25}Mg reaction. This may also be seen in Figure 20, where composition parameters in the convective shell are shown as a function of time. We have used the conservative cross section for the ^{22}Ne(α, n)^{25}Mg reaction given by Caughlan & Fowler (1988) to obtain this result. Käppeler (1995) uses the currently available experimental data on this reaction (particularly an established resonance at 828 keV) to suggest that at a temperature of 325×10^6 K the rate is at least 2.5 times the rate given by Caughlan & Fowler (1988), and at a temperature of 300×10^6 K it is at least 1.9 times larger. In the 11th pulse, the maximum temperature at the base of the convective shell is $\sim 325 \times 10^6$ K, and over most of the burning phase it is larger than $\sim 300 \times 10^6$ K. Thus, even at an early stage in the progress toward a limit cycle, one may surmise that at least $\sim$25% of the original CNO elements is converted into ^{25}Mg and neutrons. In the solar system distribution, the number abundance of ^{56}Fe is $\sim$1/40 times the number abundance of CNO elements, so approximately 10 neutrons are released for every ^{56}Fe seed. This is sufficient to ensure the production of a large overabundance of *s*-process isotopes (e.g., Truran & Iben 1977). However, because of the high neutron densities during neutron-capture nucleosynthesis, these isotopes may not be in the solar system distribution at critical branch points (Despain 1980; Busso et al. 1988; but see Cosner, Iben, & Truran 1980). For example, at the base of the convective shell, when the temperature there is 325×10^6 K, neutrons are released at the rate $\dot{n}_n \sim 4 \times 10^{13} \rho_0\ \mathrm{cm}^{-3}\ \mathrm{s}^{-1}$, where ρ_0 is the density in g s^{-1}. Choosing a mean neutron-capture cross section of $\sigma_{nc} \sim 15$ mbarns, a relative velocity of

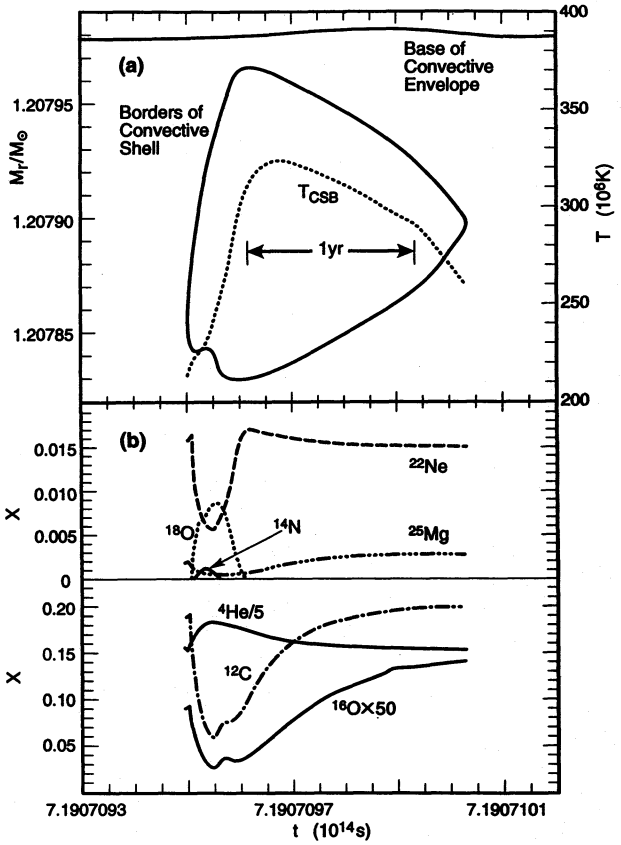

FIG. 20.—Time dependences of the border of the convective shell and the temperature T_{CSB} at the base of the shell (*upper panel*), and time dependences of composition variables (*lower panel*) during the 11th pulse.

$\sim 3 \times 10^8$ cm s^{-1}, and a mean number density of capturers as $n_c \sim (1/42)(0.019/22) \times 6.023 \times 10^{23}\ \rho_0\ \text{cm}^{-3} \sim 1.2 \times 10^{19}$, the neutron density is $n_n = \dot{n}_n/(n_c\langle\sigma_{nc}v\rangle) \sim 7 \times 10^{11}$ cm^{-3}, or $\sim$4 orders of magnitude larger than is traditionally assumed appropriate for matching the solar system distribution of *s*-process isotopes at critical branch points.

Various characteristics of a model which is in the quiescent hydrogen-burning phase midway between the 11th and 12th pulses are plotted versus r in Figure 21. An important point to make is that not all of the surface luminosity ($L_S = 5.7 \times 10^4\ L_\odot$) is due to nuclear reactions in a radiative zone. Approximately $0.4 \times 10^4\ L_\odot$ is produced by hydrogen-burning within the convective envelope (which extends outward from $r = 0.0087\ R_\odot$), and $\sim 0.3 \times 10^4\ L_\odot$ comes from the release of gravitational potential energy below the base of the hydrogen-burning shell. Thus, the rate of energy production by hydrogen-burning in radiative layers is $(L_H)_{rad} \sim 5.0 \times 10^4\ L_\odot$, or $\sim$20% larger than given by the Paczyński-Uus (PU) relationship: $L \sim 59{,}000\ L_\odot (M_{core}/M_\odot - 0.52) \sim 4.1 \times 10^4\ L_\odot$. The PU relationship (Paczyński 1970; Uus 1970) is established on the assumption that hydrogen burns only in a radiative zone and that the rate of release of gravitational potential energy is negligible.

It is well known from the literature (e.g., Uus 1973a, b; Sugimoto & Nomoto 1974; Iben 1975, 1976, 1977; Blöcker & Schönberner 1991, 1995) that the luminosity of an intermediate-mass model TPAGB star typically exceeds the PU luminosity, and that for a given core mass the interpulse luminosity increases with increasing l/H and also increases with increasing total stellar mass (see, especially, Blöcker & Schönberner 1995). We have chosen a ratio of mixing length to scale height of $l/H = 1.5$ and have kept the model mass constant.

The PU relationship is actually a very good approximation either when the mass of the hydrogen-burning envelope is small enough or when l/H is small enough (or both) that no hydrogen is burned in a convective envelope. For example, it is quite a good approximation for models which are evolving along horizontal tracks in the Hertzsprung-Russell diagram after the ejection of most of the hydrogen-burning envelope. However, as emphasized by Blöcker & Schönberner (1991), dramatic departures from the PU relationship can be achieved by suitably increasing l/H. Unfortunately, there is as yet no good theoretical or observational reason for choosing one particular value of l/H over another. The fact that AGB stars which are also long-period variables (LPVs) of magnitude brighter than $M_{bol} \sim -6$ are not carbon stars (Wood, Bessell, & Fox 1983) could be used as an argument that temperatures at the base of the convective envelope in such stars are large enough to burn carbon into nitrogen faster than it is dredged up following pulse peak; since, for a given core mass and stellar mass, the temperature at the base increases with increasing l/H, the observations could in principle be used to constrain l/H. However, these stars do not live long enough to become carbon stars even if carbon did not burn in the convective envelope (see later), so this constraint is not compelling.

The fact that most of the ZrO-rich LPVs in the Magellanic Clouds are very lithium rich (Smith & Lambert 1989, 1990; Plez, Smith, & Lambert 1993; Smith et al. 1995) has been used as a constraint on l/H, and a number of calculations (Blöcker & Schönberner 1991, 1995; Sackmann & Boothroyd 1992; Boothroyd & Sackmann 1995 and references therein) suggest that in order to achieve temperatures at the base of the convective envelope sufficiently high for the ^{3}He(α, γ)^{7}Be reaction to operate efficiently (Scalo, Despain, & Ulrich 1975), values of l/H must be chosen which are substantially larger than 1.0. If the base temperature is too high, the ^{7}Be(p, γ)^{8}B reaction can destroy much of the ^{7}Be produced before it can be convected out to low enough temperatures that the ^{7}Be(e^-, ν)^{7}Li reaction occurs more rapidly than the ^{7}Be(p, γ)^{8}B reaction ($T < 20 \times 10^6$ K). Circulation must also be such that the ^{7}Li can spend enough time at low enough temperatures ($T < 3 \times 10^6$ K) that the ^{7}Li(p, α)^{4}He reaction does not prevent the buildup of substantial quantities of ^{7}Li.

Scalo et al. (1975) examine the history of ^{7}Li at the surface of model convective envelopes as a function of the assumed temperature T_{CEB} at the base of the envelope. They find, for example, that for $T_{CEB} = 75 \times 10^6$ K in the envelope corresponding to a 5 $M_\odot$ model with an initial abundance by mass of ^{3}He of $X_3 = 10^{-4}$, the duration of the Li-superrich phase (^{7}Li/H $> 10^{-9}$) is less than $\sim 10^4$ yr. The duration of the Li-superrich episode decreases rapidly with increasing T_{CEB}. Extrapolating from the information in Figure 7 of Scalo et al. (1975), one might infer that in our model, where $X_3 \sim 10^{-5}$ initially and T_{CEB} exceeds 100×10^6 K as the limit cycle is approached, the duration of the Li-superrich phase (^{7}Li/H $> 10^{-10}$) is less than 10^3 yr. This is less than 1% of the lifetime of the TPSAGB phase, in which case most observational counterparts of our model should have no detectable Li. However, the calcu-

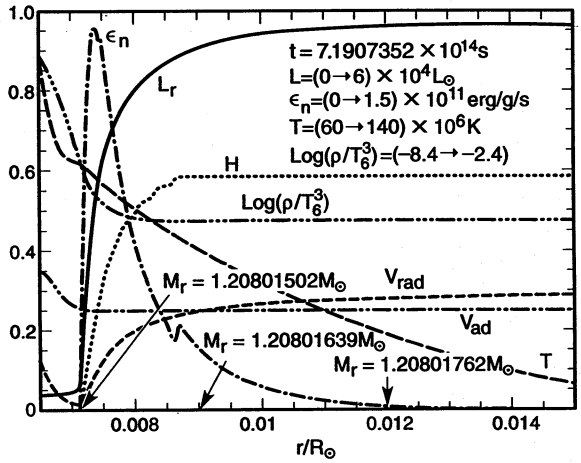

FIG. 21.—Some characteristics vs. distance r from the center of a model midway between the 11th and 12th pulses; temperature T, luminosity L_r, density ρ divided by T_6^3 ($T_6 = T/10^6$), hydrogen abundance by mass X_H (labeled as H), nuclear energy generation rate ϵ_n, radiative gradient $V_{rad} = (d \log T/d \log P)_{rad}$, and adiabatic gradient $V_{ad} = (d \log T/d \log P)_{ad}$. The scale for X_H, V_{rad}, and V_{ad} is along the left-hand axis. Scales for other variables are shown in the figure.

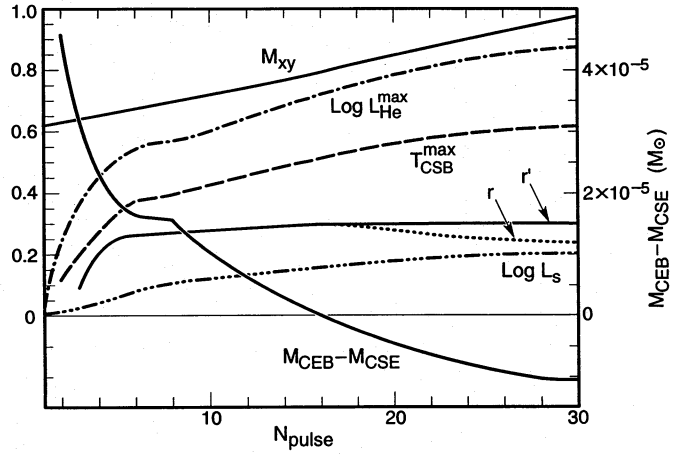

FIG. 22.—Pulse characteristics as function of pulse number: the location in mass M_{XY} of the center of the hydrogen-burning shell between pulses when L_{He} is at a relative minimum; the mean interpulse luminosity L_S; the maximum helium-burning luminosity L_{He}^{max} during a pulse; the maximum temperature T_{CSB}^{max} at the base of the convective shell; $M_{CEB} - M_{CSE}$, where M_{CEB} is the mass at the base of the convective envelope at its maximum extent inward and M_{CSE} is the mass at the outer edge of the convective shell at its maximum extent outward; and the fractional mass overlap of successive convective shells r. The variable r' is defined in the text. Scale limits are $1.202 < M_{XY}/M_\odot < 1.2102$, $4.73 < \log (L_S/L_\odot)_{max} < 5.10$, $4.5 < \log (L_{He}/L_\odot)_{max} < 6.7$, $240\text{K} < T_{CSB}^{max} < 430$ K, and $0 < r, r' < 1$.

lated lifetime of ^{3}He in the convective envelope of our model is actually $\sim 5 \times 10^4$ yr, comparable to the expected lifetime of an observational counterpart. This shows that the duration of a phase of high surface Li abundance may be a very sensitive function of the detailed structure of a model, and further exploration is justified. For the observational counterpart of our TPSAGB model, a high-Li phase could be an appreciable fraction of the TPSAGB lifetime, so we cannot flag the absence of Li as a unique signature of TPSAGB stars. ^{12}C also burns at the base of the convective envelope, with a lifetime comparable to that of ^{3}He, so the ratio of ^{12}C to ^{13}C should vary in observational counterparts from, say, ~ 25 to the equilibrium value of ~ 4.

It is evident from Figure 12 that the amplitude of the nuclear-burning luminosity variations tends to increase with each pulse cycle. The basic reason for this is the fact that layers of matter below the nuclear active region are cooling and contracting toward some equilibrium value which is unique for any given core mass. With the passage of time, the distance from the center of a point just below the helium layer is decreasing, and the gravity there is increasing. With each successive pulse, a larger input of energy is required to quench the helium-burning instability. This process continues until the thermal structure in a sufficiently large layer of matter below the nuclear active region has reached "local equilibrium"—a steady state structure which changes only very slowly at the rate at which the core mass increases secularly (e.g., Neo et al. 1977; Fujimoto & Sugimoto 1979, 1982). Once this equilibrium structure is established (for fixed core mass and fixed total mass), the pulse amplitude reaches a limit cycle which depends only on the mass of the core. The local limit-cycle interpulse surface luminosity will continue to increase as the mass of the hydrogen-exhausted core increases.

Several pulse characteristics and M_{XY}, the mass at the center of the hydrogen-burning shell at a point midway in the interpulse phase (when L_{He} is at a relative minimum), are plotted in Figure 22 versus pulse number. It is evident that the mean interpulse surface luminosity approaches a locally asymptotic value near $L_S \sim 6.4 \times 10^4\ L_\odot$ ($M_{bol} = -7.25$), which is $\sim 50\%$ larger than the PU luminosity for $M_{XY} \sim 1.21\ M_\odot$, the mass at the center of the hydrogen-burning shell when L_{He} is at a minimum between the 29th and 30th pulses. We believe that a local limit cycle has been effectively achieved, because $T_{XY} - T_{CEB}$ (where T_{XY} is the interpulse temperature at the center of the hydrogen-burning shell) has asymptotically approached a constant value (see Fig. 4 and Table 1 in Blöcker & Schönberner 1991).

Wood et al. (1992) suggest that Magellanic Cloud LPVs constrain AGB models to be less luminous than a "classical" value of $M_{bol} \sim -7.1$ ($L \sim 5.6 \times 10^4\ L_\odot$). Their argument rests on the choice of a distance modulus of 18.5 mag for the LMC and of 18.9 mag for the SMC, and on the belief that two IR sources in the LMC with no detected OH maser emission and with estimated magnitudes of $M_{bol} = -7.30$ ($L \sim 6.7 \times 10^4\ L_\odot$) (IRAS 04509−6922) and $M_{bol} = -7.62$ ($L \sim 9.0 \times 10^4\ L_\odot$) (IRAS 04530−6916) are not really AGB stars. From our perspective, the evidence supports membership in the AGB class. The band of stars labeled "AGB stars" in Figure 8 of Wood et al. (1992) is widely separated from the band labeled supergiants in this figure, and the eight IR stars form a clear extension of the AGB band defined by optical sources. The dispersion in luminosity of the eight IR sources (including the three sources without detected OH emission) is comparable to that of optical sources at smaller periods. The small statistics do not permit one to infer (as Wood et al. 1992 do) that there is a sharp cutoff in the luminosity function at $M_{bol} \sim -7.1$. For example, constructing a luminosity function for all of the stars in the AGB band (including all eight IR sources), one finds as sharp a gap in the distribution of optical sources at $M_{bol} \sim -5.8$ as there is in the distribution of IR sources at $M_{bol} \sim -7.1$..

Theoretical models made over the past two decades have the property of exceeding the classical limit (by an amount which depends on the choice of l/H and other input physics), so the classical limit is not a hard limit, although it

remains a useful benchmark. Parenthetically, for TPSAGB stars the effective Chandrasekhar mass is 1.37 $M_\odot$ (Nomoto 1987), and the PU relationship gives for the classical limit $L = 5.0 \times 10^4$ $L_\odot$ or $M_{bol} = -7.0$. Our model, with $M_{bol} \sim -7.25$, has the same luminosity as IRAS 04509−6922.

The temperature T_{CSB} at the base of the convective shell during pulse peak approaches ~360 K (Fig. 22). As is demonstrated in Figure 23, which describes nucleosynthesis in the convective shell during the 30th pulse, temperatures within the convective shell remain large enough so that the $^{22}Ne(\alpha, n)^{25}Mg$ reaction destroys about half of the ^{22}Ne incorporated in the convective shell, providing ~20 neutrons for every ^{56}Fe seed nucleus. Had we chosen a cross section for the neutron source 2.5 times larger, as suggested by Käppeler (1995), approximately 80% of the ^{22}Ne would be converted into ^{25}Mg and neutrons, providing ~30 neutrons per iron seed. Choosing $\sigma_{BC} \sim 15$ mbarns and repeating the exercise performed in the case of the 11th pulse, we find that at the base of the convective shell when $T_{CSB} = 358 \times 10^6$ K, the neutron density is $n_n \sim 6 \times 10^{12}$ cm^{-3}. According to current wisdom, departures from the solar system distribution of *s*-process isotopes at critical branch points are expected to be even larger than in the 11th pulse.

The "third" dredge-up process (e.g., Iben 1975) occurs during pulse powerdown for all pulses in which a convective shell is formed. In this process, the base of the convective envelope extends inward in mass beyond the location of the hydrogen profile into a region where there are, first, products of complete hydrogen-burning and then products of partial helium-burning. After the 16th pulse, carbon-rich and *s*-process–rich matter is dredged into the convective envelope. This is shown in Figure 22 by the variable $M_{CEB} - M_{CSE}$, where M_{CEB} is the mass at the base of the convective envelope at minimum and M_{CSE} is the mass at the outer edge of the convective shell at maximum. In pulses 29 and 30, ΔM_{CS} (the mass of the convective shell at maximum extension) = 1.555×10^{-4} and the amount of carbon-rich matter dredged up is $\Delta M_{dg} = M_{CSE} - M_{CEB} = 0.068 \Delta M_{CS} = 1.066 \times 10^{-5}$. The amount of mass processed by hydrogen-burning between pulses is $\Delta M_H = 1.257 \times 10^{-4}$ $M_\odot$. The mass between the outer edge of the convective shell (at maximum mass) and the base of the convective envelope (just prior to a shell flash) is $\Delta M_{EB} = 6.44 \times 10^{-6}$ $M_\odot$ (see Fig. 23). These numbers give $\Delta M_H = \Delta M_{XY} + \Delta M_{dg} + \Delta M_{EB} = 1.086 \times 10^{-4} + 1.066 \times 10^{-5} + 6.4 \times 10^{-6} = 1.257 \times 10^{-4}$.

Shown in Figure 24 are the mass M_{XY} at the center of the hydrogen-burning shell [defined as the point where $X(^1H)$ is one-half the surface value] and the mass boundaries of the convective shells formed during the 29th and 30th pulses. The mass overlap "*r*" of successive convective shells, which plays a role in determining the asymptotic distribution of *s*-process isotopes that are made after many pulses (e.g., Ulrich 1973; Truran & Iben 1977), is defined graphically in Figure 24. The limit-cycle value of *r* is ~0.24 (Fig. 22). Also shown in Figure 22 is $r' = r + \Delta M_{dg}/\Delta M_{CS}$, the value of *r* if the dredge-up of hydrogen-free matter did not occur.

The third dredge-up phenomenon is essentially identical to the second dredge-up phenomenon. Energy leaks out of a region where it is produced at a high rate by nuclear reactions; a large fraction of this energy is absorbed by the radiative zone between the energy source and the base of the convective layer, forcing matter in this zone to expand and cool; the increase in luminosity flux at the base of the convective envelope forces the base to move inward in mass.

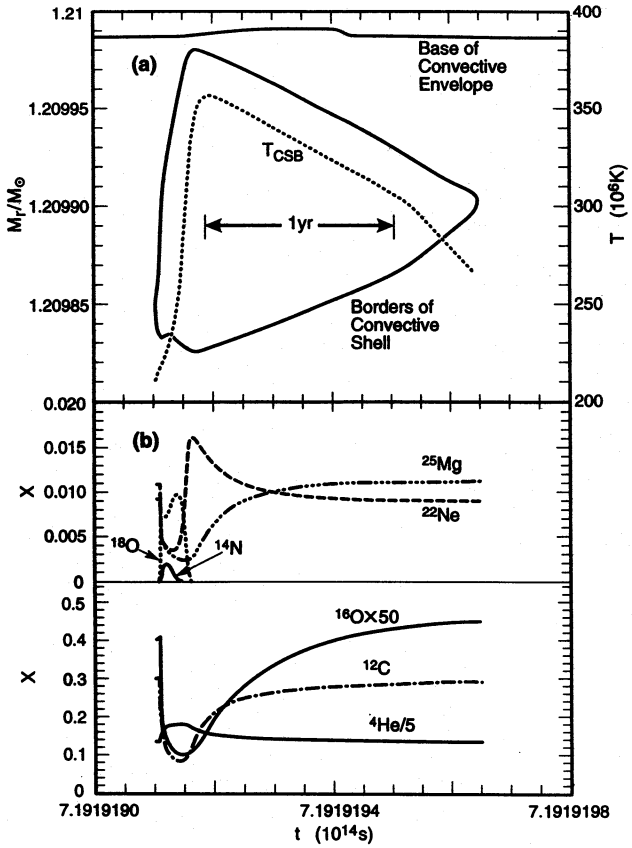

FIG. 23.—Same characteristics vs. time as in Fig. 20, but for the 30th pulse.

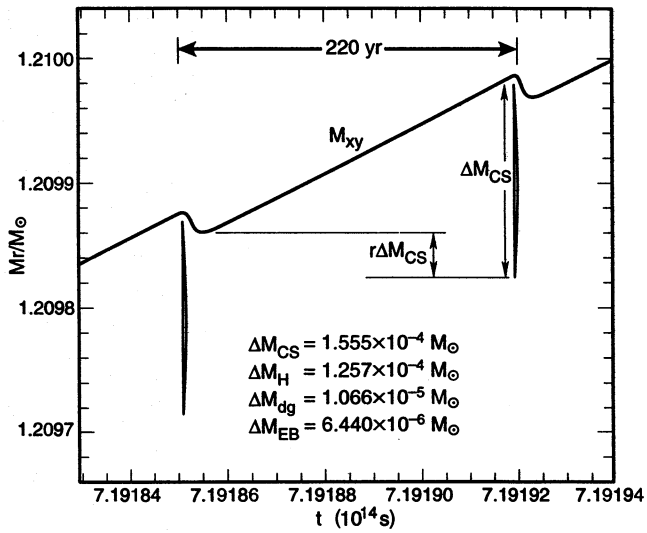

FIG. 24.—Time dependence of the mass M_{XY} of the center of the hydrogen-burning shell from before the 29th pulse to after the 30th pulse. Also given are the borders of the 29th and 30th convective shells and a definition of overlap *r*, where ΔM_{CS} is the maximum mass of the convective shell. In the figure are given the values of ΔM_{CS}, ΔM_H (the mass through which the hydrogen profile moves between pulses), ΔM_{dg} (the amount of mass dredged up during pulse powerdown), and ΔM_{EB} (the mass between the outer edge of the convective shell [at maximum extent] and the base of the convective envelope).

The process stops when the luminosity at the base of the absorbing radiative zone and the mass of the absorbing zone decrease below critical values. When convective overshoot is not invoked, the rate at which $M_{CEB} - M_{CSE}$ decreases with pulse number becomes very small in the sixth through eighth pulses. Therefore, beginning with the ninth pulse, we have taken overshoot into account following Iben (1976). Using the estimate given by the mixing-length theory for the velocity v_c of convective elements near the base of the convective envelope, overshoot is assumed to mix material from the fully convective region into the formally convectively stable region along a front which moves with a spatial speed $v_f = \Delta r/\tau_{mix}$, where $\Delta r = v_c^2/2g$ is the characteristic distance traveled by the overshooting convective elements before being stopped by the buoyancy force, $\tau_{mix} = H_P/v_c$ is the characteristic mixing time at the base of the fully convective zone, and H_P is the pressure scale height. With this recipe, the base of the convective envelope at the end of the dredge-up phase extends about one pressure scale height deeper than when overshoot is neglected. The degree of overshoot could be much larger than we have calculated.

Because of the large average mass of the envelope and the small degree of dredge-up which we estimate, the enhancement in the abundances of CNO elements and neutron-rich isotopes due to dredge-up will not be very dramatic over most of the lifetime of the observational counterpart of our model. In 500 pulse cycles, the total amount of carbon dredged up is only $\sim 1.5 \times 10^{-3}\ M_\odot$, compared with the $\sim 1.6 \times 10^{-2}\ M_\odot$ of carbon in the envelope immediately after the second dredge-up episode (see § 2). Assuming an enhancement of neutron-rich isotopes in the convective shell of $\sim 10^2$–10^3 relative to solar (e.g., Truran & Iben 1977) and an average envelope mass of $\sim 4\ M_\odot$, neutron-rich isotopes in the envelope will be enhanced by at most a factor of ~ 1.1–2.7, an enhancement which may not be particularly noticeable. An estimate of the degree of dredge-up depends on the treatment of convection in the outer parts of the convective envelope where the superadiabatic gradient is large (e.g., on the choice of l/H if a mixing-length algorithm is assumed), and it is very sensitive to the treatment of overshoot at the base of the convective envelope. Thus, if the observations eventually uncover, e.g., a factor of 10 enhancement of neutron-rich isotopes in a nonsolar distribution, this would imply a degree of dredge-up at least ~ 6 times larger than we have estimated, a result which we would not find at all surprising.

The local limit-cycle characteristics we have calculated may be compared with those estimated by interpolating between the characteristics of two 7 $M_\odot$ models for which the pulse instability has been suppressed until the hydrogen-exhausted core mass has reached the values of 1.16 and 1.36 $M_\odot$, respectively, at which point evolution is followed until one thermal pulse takes place (Iben 1977). The results are shown in Table 1, where $\Delta n_{22}/n_{22}^0$ is the fraction of initial ^{22}Ne destroyed. It is evident that the first pulse which occurs after the pulse-suppression mechanism is suspended is more vigorous than the limit-cycle pulse. From the point of view of the observations, the most important difference is that temperatures in the convective shell are smaller in the limit-cycle case than in the "instability-suppression, one-pulse" approximation, with the result that fewer neutrons per iron seed are produced.

TABLE 1

CHARACTERISTICS OF A LIMIT-CYCLE PULSE[a]

Variable	Estimated	Calculated
$L_S/L_\odot$	7.2×10^4	6.4×10^4
$L_{He}^{max}/L_\odot$	5.6×10^6	2.7×10^6
$\Delta M_{CS}/M_\odot$	2.24×10^{-4}	1.56×10^{-4}
T_{CSB}/K	380	360
r	0.25	0.24
$\Delta n_{22}/n_{22}^0$	0.97	0.56

[a] Estimated and calculated characteristics of a limit-cycle pulse ($M_{core} = 1.21\ M_\odot$) are from Iben 1977 and this paper, respectively.

4. SUMMARY AND DISCUSSION

We have followed the evolution of a 10 $M_\odot$ model star of Population I composition from the main sequence, through the core carbon-burning stage as it forms an electron-degenerate ONe core, and into the TPSAGB stage.

Two important errors which affected results in Paper I have been corrected. The final mass of the ONe core decreases from the 1.3 $M_\odot$ found in Paper I to 1.2 $M_\odot$, and details of abundance distributions in the core differ from those found in Paper I. In agreement with Paper I, ^{23}Na is more abundant than ^{24}Mg over most of the ONe interior, a result which has possible ramifications for the collapse of accreting ONe white dwarfs. The carbon-burning network has been enlarged by a factor of ~ 2 over that used in Paper I, but the only new isotope made in interesting quantities is ^{27}Al. For future studies of carbon-burning in models of initial mass in the range 9–11 $M_\odot$, we recommend use of the network adopted in Paper I, with the addition of ^{27}Al, ^{28}Al, and ^{28}Si and the deletion of ^{23}Mg.

Carbon-burning is ignited off center and proceeds by a series of flashes which force the development of a convective shell. The convective shell persists during a subsequent quiescent carbon-burning phase. Except after the second flash, the base of the convective shell moves outward in mass. After the second flash, the base of the convective shell progresses toward the center, and the spatial velocity with which the carbon-burning "flame" moves toward the center can be described by a theory of flame fronts developed by Timmes & Woosley (1992) and Timmes et al. (1994). In this theory it is assumed that the rate of nuclear energy generation in the flame equals the rate of neutrino losses from the convective shell. In our calculations, this condition is met within a factor of 2 during the progress of the flame toward the center, but it is not met during the bulk of the carbon-burning phase. We resolve the inward-moving flame front by choosing zones of spatial thickness ~ 0.2 km.

The second dredge-up phenomenon occurs near the end of the carbon-burning phase, and the correlation between the surface luminosity and the surface radius can be understood quantitatively as a consequence of a deep convective envelope which is "transparent" to the radiation impinging from below and an atmosphere in which the H^- ion is the dominant source of opacity. As the carbon-burning shell approaches the helium-burning shell, the carbon-burning luminosity makes a contribution to the occurrence of the second dredge-up phenomenon. Because of decreasing absorption between the two burning shells, the luminosity at the edge of the helium-burning shell increases, even as

both the carbon-burning luminosity and the helium-burning luminosity decrease.

Hydrogen is reignited at the end of the second dredge-up phase. During the first five thermal pulses, the carbon-burning luminosity drops below 1 $L_{\odot}$, and it tends toward zero thereafter. No further carbon-burning flashes occur.

The composition of the core at the end of carbon-burning has relevance for the evolution of CVs and for the composition characteristics of associated classical novae. If the real counterpart of the model we have studied is in a binary with a low-mass main-sequence companion, and if it fills its Roche lobe during or after the second dredge-up phase (as its radius increases from 375 to 600 $R_{\odot}$), a common envelope will form, and any small amount of hydrogen-rich and helium-rich material that remains above the ONe core of the primary following the completion of the common envelope phase will be lost in a radiative wind. When the secondary comes into contact with its Roche lobe (due to orbital angular momentum loss mediated by a magnetic stellar wind or by gravitational wave radiation), hydrogen-rich material falls onto a "bare" white dwarf. Contrary to common belief, the subsequent nova explosions will not at first be Ne rich, because the outer 0.01 $M_{\odot}$ of the bare core is composed primarily of O and C, the dominant trace isotope being ^{25}Mg; there are essentially no Ne isotopes. Ne will appear in nova ejecta only after $\sim 10^3$ outbursts have occurred and the Ne-free layer has been removed.

The original primary objective of this paper was to follow the thermal pulses of AGB models with ONe cores (SAGB models), and this we have accomplished. The limit-cycle characteristics of the pulses are established after approximately 30 pulse cycles have been computed. Limit-cycle values are mean interpulse luminosity $L_S \sim 6.4 \times 10^4\ L_{\odot}$ ($M_{\rm bol} = -7.25$), maximum helium-burning luminosity $L_{\rm He}^{\rm max} \sim 2.7 \times 10^6\ L_{\odot}$, maximum temperature at the base of the convective shell $T_{\rm CSB}^{\rm max} \sim 360 \times 10^6$ K, mass overlap of successive convective shells $r \sim 0.24$, and fraction of matter once contained in the convective shell that is dredged up during pulse powerdown $\lambda = \Delta M_{\rm dg}/\Delta M_{\rm CS} \sim 0.07$. L_S is $\sim$50% larger than the luminosity given by the PU relationship. The reason for this difference in luminosities—hydrogen-burning in the convective zone above the radiative hydrogen-burning layer—is well known and is quantitatively dependent on the choice of l/H as well as on the mass of the star. We have chosen $l/H = 1.5$.

We find that temperatures in the convective shell during a helium-shell flash become large enough for a long enough time that the ^{22}Ne(α, n)^{25}Mg reaction becomes a potent source of neutrons with 20–30 neutrons being released for every iron-seed nucleus, depending on the choice of cross section for the (α, n) reaction. However, according to many authors, the neutron densities (typically 6×10^{12} cm^{-3}) are far too large for the production of s-process isotopes in the solar system distribution, especially near critical branch points.

The LPVs in the Magellanic Clouds which are not carbon stars show excesses of ZrO (Wood et al. 1983) and are Li superrich (Smith & Lambert 1989, 1990; Plez et al. 1993; Smith et al. 1995). Since Zr is an s-process isotope and the Li-superrich phenomenon is a consequence of high temperatures at the base of a convective envelope surrounding an electron-degenerate core (Scalo et al. 1975; Sackmann & Boothroyd (1992); Boothroyd & Sackmann 1995 and references therein), these LPVs must be thermally pulsing AGB or SAGB stars. Some of the most luminous LPVs should have progenitors as massive as 10 $M_{\odot}$. These might be expected to show s-process distributions which are nonsolar and abundance mixes of Mg isotopes which are distinctly nonsolar (see Lambert 1991). If none show such anomalies, this could mean that the cross section for the ^{22}Ne(α, n)^{26}Mg reaction is considerably smaller than currently estimated (Käppeler 1995) and that some neutron source other than ^{22}Ne is producing Zr. On the other hand, it is equally possible that, because of their initially massive envelopes and short lifetimes, typical TPSAGB stars simply do not develop detectable overabundances of either carbon or s-process isotopes until near the end of their lives, when their envelope masses have become suitably small. By then, however, superwind matter possibly masks the optical source. Because there is a fairly large abundance of ^{3}He in the envelope of an SAGB star [$X(^3\text{He}) \sim 10^{-5}$ after the second dredge-up episode in our 10 $M_{\odot}$ model], observational counterparts may experience a Li-superrich phase. Because the rate of burning ^{3}He is similar to that of burning ^{12}C, Li-rich stars will have small ^{12}C/^{13}C ratios and may also be carbon poor (C < O), provided the third dredge-up mechanism is not too effective at injecting fresh carbon into the convective envelope. Thus, the signature of a TPSAGB star during the first part of its life may be C < N < O, ZrO normal, and Li/H greater than "solar" (Li/H $\sim 10^{-10}$). During the last part of its life, one might expect Li/H less than solar, and, if ZrO is significantly larger than solar, Mg isotopes should be in distinctly nonsolar ratios, and there may be departures from solar in the distribution of heavy s-process isotopes at critical branch points.

In all cases, TPSAGB stars define the brightest segment of the AGB band, and brightnesses in excess of $M_{\rm bol} = -7.1$ are expected to be common. The two IR stars IRAS 04509−6922 ($M_{\rm bol} = -7.3$) and IRAS 04530−6916 ($M_{\rm bol} = -7.6$) in the LMC (Wood et al. 1993) and the two Li-superrich stars HV 838 and HV 1963 (both with $M_{\rm bol} \sim -7.2$) in the SMC (Smith et al. 1995) may be TPSAGB stars. Betelgeuse, with a luminosity of $\sim 6.3 \times 10^4\ L_{\odot}$ ($M_{\rm bol} = -7.2$), may be a TPSAGB star. Lambert et al. (1984) find that ^{12}C/^{13}C = 6 ± 1, and that abundances by number of CNO elements are related by (C:N:O) = (2.21:5.43:5.21). The CNO abundance ratios indicate that matter in the envelope of Betelgeuse has experienced considerable carbon-burning. However, the ratio of ^{12}C to ^{13}C is so close to the equilibrium ratio of $\sim$4 that it is surprising that the relative abundance of C is as large as it is, unless substantial dredge-up of carbon has occurred. The fact that Betelgeuse is not Li superrich is consistent with the fact that the lifetime of ^{3}He is essentially the same as the lifetime of ^{12}C in the convective envelope of an intermediate-mass star. Since considerable ^{12}C has been burned, a Li-superrich phase may have come and gone.

At the surface of our initial model, (C:N:O) = (3.56:1.00:7.97) and, just after the model has completed the second dredge-up phase, (C:N:O) = (2.35:4.25:6.26), which is not unlike the abundance ratios for Betelgeuse. However, ^{12}C does burn during the thermally pulsing phase, and if the third dredge-up phenomenon did not occur, the ratio of C to N would decrease monotonically to the equilibrium value. For example, when half of the initial ^{12}C in the envelope has been burned, the model would have (C:N:O) $\sim$ (1.17:5.43:6.26). But dredge-up does occur, although our explicit estimate of the degree of dredge-up

($\lambda = 0.07$) is only a lower limit. An estimate of λ can be attempted by comparing with the observations. Let the amount of matter dredged up after each pulse be $\lambda\Delta M_{CS}$ and let the normalized abundance of ^{12}C by number in the matter dredged up be $\sim(0.25/12)15{,}000 = 313$. The normalization factor of 15,000 converts the actual abundance by number to an abundance relative to nitrogen in the initial model. If no mass loss and no envelope burning occurred, the number abundance of ^{12}C in the convective envelope after N_p pulses would increase by $\Delta C_{dg} \sim (N_p\lambda\Delta M_{CS}/8.8\ M_\odot)313 \sim N_p\lambda(1.56 \times 10^{-4}/8.8)313 = 0.00555N_p\lambda$. After, say, 500 pulses, $\Delta C_{dg} \sim 3\lambda$. Thus, to make up for the fact that ^{12}C is actually burning in the envelope, λ would have to be of the order of 0.3 or larger.

We realize that our interpretation is somewhat strained. Betelgeuse is not a large-amplitude LPV as we are accustomed to thinking TPAGB stars should be, and it is currently losing mass at the very modest rate of $\sim 10^{-6}\ M_\odot\ yr^{-1}$ (see de Jager, Nieuwenhuijzen, & van der Hucht 1988 and references therein). In comparing the observed abundance ratios with the theoretical abundance ratios, we have made the unsubstantiated assumption that the initial C/N ratio in Betelgeuse is solar, and we have ignored the uncertainties in observed abundance estimates. The large degree of dredge-up we infer implies an overabundance of *s*-process isotopes by a factor in the range 1.6–7 and an anomalous distribution of these isotopes. To our knowledge, no enhancements or indications of anomalous distributions have been reported. On the other hand, we are aware of no mechanism other than rotationally induced mixing during the main-sequence phase whereby a massive star (which avoids the AGB phase) can produce the $^{12}C/^{13}C$ ratio found for Betelgeuse. Since there appears to be no evidence that such mixing occurs in B-type main-sequence stars of luminosities comparable to that of Betelgeuse (Cunha & Lambert 1994), we are left with yet another mystery.

If the real counterpart of our model is a single star, nuclear burning will increase the mass of a CO layer above the ONe interior to $\sim 0.06\ M_\odot$ before the hydrogen-rich surface has been effectively removed by a superwind. The star becomes the $\sim 1.26\ M_\odot$ central star of a planetary nebula at a luminosity of $\sim 4.4 \times 10^4\ L_\odot$ (as given by the PU relationship); it loses, via a radiative wind, any surface hydrogen and helium remaining and, thanks to diffusion, eventually evolves into a non-DA white dwarf with a surface composition which is predominantly carbon.

We thank the National Center for Supercomputing Applications at the University of Illinois and the Centre de Supercomputació de Catalunya for providing computational facilities.

REFERENCES

Arnett, W. D. 1969, Ap&SS, 5, 180
———. 1973, ApJ, 179, 249
Arnett, W. D., & Truran, 1969, ApJ, 157, 339
Becker, S. A., & Iben, I., Jr. 1979, ApJ, 232, 831
———. 1980, ApJ, 237, 111
Blöcker, T., & Schönberner, D. 1991, A&A, 244, L43
———. 1995, in Nuclei in the Cosmos III, ed. M. Busso, R. Gallino, & C. M. Raiteri (New York: AIP), 399
Boothroyd, A. I., & Sackmann, J. 1995, Mem. Soc. Astron. Italiana, in press
Boozer, A. H., Joss, P. C., & Salpeter, E. E. 1973, ApJ, 181, 393
Busso, M., Picchio, G., Gallino, R., & Chieffi, A. 1988, ApJ, 326, 196
Caughlan, G. R., & Fowler, W. A. 1988, At. Data Nucl. Data Tables, 40, 283
Canal, R., Isern, J., & Labay, J. 1992, ApJ, 398, L49
Cosner, K., Iben, I., Jr., & Truran, J. W. 1980, ApJ, 238, L91
Cunha, K., & Lambert, D. L. 1994, ApJ, 426, 170
de Jager, C., Nieuwenhuijzen, H., & van der Hucht, K. A. 1988, A&AS, 72, 259
Despain, K. H. 1980, ApJ, 236, L165
Dominguez, I., Tornambè, A., & Isern, J. 1993, ApJ, 419, 268
Finzi, A., & Wolf, R. A. 1967, ApJ, 150, 115
Fujimoto, M. Y., & Iben, I., Jr. 1992, ApJ, 399, 646
Fujimoto, M. Y., & Sugimoto, D. 1979, PASJ, 31, 1
———. 1982, ApJ, 257, 291
García-Berro, E., & Iben, I., Jr. 1994, ApJ, 434, 306 (Paper I)
García-Berro, E., Ritossa, C., & Iben, I., Jr. 1995, in preparation (Paper III)
Gutiérrez, J. 1996, in Thermonuclear Supernovae, ed. R. Canal, J. Isern, & P. Ruez-Lapuente (Dordrecht: Kluwer), in press
Gutiérrez, J., García-Berro, E., Iben, I., Jr., Isern, J., Labay, J., & Canal, R. 1996, ApJ, in press
Hansen, C. J., & Kawaler, S. D. 1994, Stellar Interiors (New York: Springer)
Hashimoto, M., Iwamoto, K., & Nomoto, K. 1993, ApJ, 414, L105
Iben, I., Jr. 1975, ApJ, 196, 525
———. 1976, ApJ, 208, 165
———. 1977, ApJ, 217, 788
———. 1982, ApJ, 259, 244
———. 1991, ApJS, 76, 55
Iben, I., Jr., Fujimoto, M. Y., & MacDonald, J. 1992, ApJ, 388, 521
Iben, I., Jr., & Tutukov, A. V. 1984, ApJS, 54, 335
———. 1985, ApJS, 58, 661
———. 1989, ApJ, 342, 430
———. 1996, ApJS, in press
Käppeler, F. 1995, in Nuclei in the Cosmos, ed. M. Busso, R. Gallino, & C. M. Raiteri (New York: AIP), 101
Lamb, S. A., Howard, W. M., Truran, J. M., & Iben, I., Jr., 1977, ApJ, 217, 213
Lamb, S. A., Iben, I., Jr., & Howard, W. M. 1975, ApJ, 207, 209
Lambert, D. L. 1991, in Evolution of Stars: the Photospheric Abundance Connection, ed. G. Michaud & A. Tutukov (Dordrecht: Kluwer), 299
Lambert, D. L., Brown, J. A., Hinkle, K. H., & Johnson, H. R. 1984, ApJ, 284, 223
Lyne, A. G., Biggs, J. D., Harrison, P. A., & Bailes, M. 1993, Nature, 361, 47
Miyaji, S., & Nomoto, K. 1987, ApJ, 318, 307
Miyaji, S., Nomoto, K., Yokoi, K., & Sugimoto, D. 1980, PASJ, 32, 303
———. 1960, Soviet Astron., 3, 744
Neo, S., Miyaji, S., Nomoto, K., Sugimoto, D. 1977, PASJ, 29, 249
Nomoto, K. 1984, ApJ, 277, 791
———. 1987, ApJ, 322, 206
Paczyński, B. 1970, Acta Astron., 20, 47
Plez, B., Smith, V. V., & Lambert, D. L. 1993, ApJ, 418, 812
Rakavy, G., Shaviv, G., & Zinamon, Z. 1967, ApJ, 150, 131
Sackmann, I.-J., & Boothroyd, A. I., ApJ, 392, L71
Scalo, J. M., Despain, K. H., & Ulrich, R. K. 1975, ApJ, 196, 805
Schwartzman, E., Kovetz, A., & Prialnik, D. 1994, MNRAS, 269, 323
Schwarzschild, M., & Härm, R. 1965, ApJ, 142, 855
Smith, V. V., Plez., B., Lambert, D. L., & Lubowich, D. A. 1995, ApJ, 441, 735
Smith, V. V., & Lambert, D. L. 1989, ApJ, 345, L75
———. 1990, ApJ, 361, L69
Sugimoto, D., & Nomoto, K. 1974, in Late Stages of Stellar Evolution, ed. R. J. Taylor (Dordrecht: Reidel), 105
———. 1975, PASJ, 27, 197
Timmes, F. X., & Woosley, S. E. 1992, ApJ, 396, 649
Timmes, F. X., Woosley, S. E., & Taam, R. E. 1994, ApJ, 420, 348
Truran, J. W., & Iben, I., Jr. 1977, ApJ, 216, 797
Ulrich, R. K. 1973, in Explosive Nucleosynthesis, ed. D. N. Schramm & W. D. Arnett (Austin: Univ. Texas Press), 139
Uus, U. 1970, Nauchn. Inf., 17, 48
———. 1973a, Nauchn. Inf., 26, 83
———. 1973b, Nauchn. Inf., 26, 96
Weigert, A. 1966, Z. Astrophys., 64, 395
Wijers, R. M. A. J., & Paczyński, B. 1993, ApJ, 415, L115
Wood, P. R., Whiteoak, J. B., Hughes, S. M. G., Bessell, M. S., Gardner, F. F., & Highland, A. R. 1992, ApJ, 397, 552
Wood, P. R., Bessell, M. S., & Fox, M. W. 1983, ApJ, 272, 99